Available online at BCREC website: https://bcrec.id

Bulletin of Chemical Reaction Engineering & Catalysis, 16 (4) 2021, 773-795

Research Article

# The Dependency of Kinetic Parameters as a Function of Initial Solute Concentration: New Insight from Adsorption of Dye and Heavy Metals onto Humic-Like Modified Adsorbents

**Rahmat Basuki[1,2], Bambang Rusdiarso[2,*], Sri Juari Santosa[2], Dwi Siswanta[2]**

*[1]Department of Chemistry, Universitas Pertahanan RI, Bogor, 16810, Indonesia.*
*[2]Department of Chemistry, Universitas Gadjah Mada, Yogyakarta 55281, Indonesia.*

*Received: 25th July 2021; Revised: 12nd August 2021; Accepted: 12th August 2021*
*Available online: 14th August 2021; Published regularly: December 2021*

## Abstract

Kinetics parameters are the essential issue in the design of water treatment systems for pollutants uptake. Though numerous studies have identified the boundary conditions that exert influence on the kinetics parameters, the influence of the dynamic initial solute concentration ($C_0$) to the kinetic parameters generated from fitting kinetics model to experimental data has not been investigated thoroughly. This study revealed a change in the kinetics parameter value due to changes in the adsorption mechanism as an effect of dynamic $C_0$. It was observed that at higher $C_0$ the adsorbed solute at equilibrium ($q_e$) increases and it takes longer time to reach equilibrium. As a result, the kinetics rate constant ($k$) calculated from adsorption reaction model (Lagergren, Ho, Santosa, and RBS) was decreased. In general, Ho model exhibit higher correlation coefficient value ($R^2$) among the other model at low $C_0$. At high $C_0$, Ho's $R^2$ tend to decrease while the Lagergren and RBS's $R^2$ was increased. The amendment mechanism from external mass transport to intra-particle diffusion as a rate limiting step was evidenced by Boyd and Weber-Morris kinetics model. Further, the physicochemical properties of the adsorbent used in this work: chitin and $Fe_3O_4$ modified horse dung humic acid (HDHA-$Fe_3O_4$ and HDHA-Ch, respectively) with the solute: Pb(II), Methylene Blue (MB), and Ni(II) was deeply discussed in this paper. The outcomes of this work are of prime significance for effective and optimum design for pollutant uptake by adsorption equipment.



***Keywords***: Adsorption; Heavy Metals and Dye; Humic-Like Modified Adsorbent; Initial Solute Concentration; Kinetics Parameter Dependency

***How to Cite***: R. Basuki, B. Rusdiarso, S.J. Santosa, D. Siswanta (2021). The Dependency of Kinetic Parameters as a Function of Initial Solute Concentration: New Insight from Adsorption of Dye and Heavy Metals onto Humic-Like Modified Adsorbents. *Bulletin of Chemical Reaction Engineering & Catalysis*, 16(4), 773-795 (doi:10.9767/bcrec.16.4.11816.773-795)

***Permalink/DOI***: https://doi.org/10.9767/bcrec.16.4.11816.773-795

## 1. Introduction

Adsorption is one of the most widely methods for contaminant removal from aqueous polluted medias [1,2]. Concerning adsorption issues, thermodynamics and kinetics aspect should be involved to obtain more details about its performance and mechanisms. Besides for adsorption capacity, kinetics performance of a particular adsorbent is also great significance for the pilot application. From kinetics study, the solute uptake rate, which determines time-dependent completion of adsorption reaction, may be established. Furthermore, the scale of an adsorption apparatus can be determined based on kinetics

* Corresponding Author.
Email: brusdi_mipa@ugm.ac.id (B. Rusdiarso);
Telp: +62 815-6860-897, Fax: +62- 274-545188

information [3]. In general, adsorption kinetics is the base to determine the performance of fixed-bed or any other flow-through systems.

In the past two decades, several mathematics models have been proposed to describe the empirical adsorption data. The proposed kinetics models ordinarily classified as adsorption reaction and adsorption diffusion models. Both models are widely applied to describe the kinetics process of adsorption, even though they are quite different in point of view. Adsorption diffusion models were constructed on the basis of three consecutive steps [4]: external diffusion, internal or intra-particle diffusion, and adsorption-desorption between solute and active sites of an adsorbent (mass action). Whereas, adsorption reaction models rising from chemical reaction kinetics was based on the entire process of adsorption without considering the steps mentioned in adsorption diffusion models.

Adsorption diffusion models assumed that mass action is a very fast process and can be negligible for kinetics study so the rate limiting steps is always controlled by liquid film diffusion or intraparticle diffusion [4]. The well-known adsorption diffusion models that widely applied in adsorption study are film diffusion mass transfer rate equation model and Weber-Morris intraparticle model [5,6]. The diffusion mass transfer rate equation model presented by Boyd *et al*. [7] is:

$$B_t = -0.4977 - \ln(1-F) \quad (1)$$

where, $F$ represent the fraction of solute adsorbed at any time, $t$ (min) as calculated by $F = q_t/q_e$. Weber-Morris found that in many adsorption cases, the adsorbed solute varies almost proportionally with the $t^{1/2}$ rather than contact time $t$ [6]:

$$q_t = k_{\text{int}} t^{1/2} + C_i \quad (2)$$

where the $k_{\text{int}}$ (mol/g min$^{1/2}$) is the intraparticle diffusion rate. The plot of $q_t$ vs. $t^{1/2}$ shall be straight line with a slope $k_{\text{int}}$ when the intraparticle diffusion is a rate limiting step.

On the other hand, the two of most widely applied kinetics adsorption reaction models were developed by Lagergren [8] and Ho [9]. Lagergren published a first-order rate equation to describe the kinetics process of liquid-solid phase of malonic and oxalic acid onto charcoal, which is believed to be earliest kinetics models based on the adsorption equilibrium [10]. Lagergren model originated from view:

$$\frac{dq_t}{dt} = k_{Lag}(q_e - q_t) \quad (3)$$

by integrating Eq. (3) with the boundary $q_t$=0 at $t$=0, and $q_t$=$q_t$ at $t$=$t$ yields:

$$\ln(q_e - q_t) = \ln q_e - k_{Lag} t \quad (4)$$

In 1998, Ho described a kinetic process of the adsorption of divalent metal ions onto peat [9], in which the chemical bonding among divalent metal ions and polar functional groups on peat. The main assumptions were that the adsorption may be second-order and the expression given as

$$\frac{dq_t}{dt} = k_{Ho}(q_e - q_t)^2 \quad (5)$$

Integrating Eq. (5) with the boundary $q_t$=0 at $t$=0, and $q_t$=$q_t$ at $t$=$t$ yields linear form:

$$\frac{t}{q_t} = \frac{1}{k_{Ho} q_e^2} + \frac{1}{q_e} t \quad (6)$$

To distinguish kinetic equations based on adsorption equilibrium from solution concentration, Lagergren's first order and Ho's second order rate equation has been called pseudo-first-order (PFO) and pseudo-second-order (PSO), respectively [10].

However, since past decade, the problem was existed: PSO rate equation based on chemical adsorption was unsuitably applied to describe organic pollutants adsorption onto several nonpolar polymeric adsorbents (essentially a process of physical adsorption) [11]. In addition, PFO models were still widely applied to data modeling, though no adsorption mechanisms could be reasonably available. Consequently, some famous journals like *J. Hazard. Mater.* and *Sep. Purif. Technol.* began to "aware" on adsorption manuscripts based on unsuitable or simple kinetic modeling [12] and paid more attention to their boundary conditions. Azizian [13] summarized the adsorption data in literatures, and concluded that initial solute concentration ($C_0$) was greatly affect the fitting kinetics model to experimental data. When the $C_0$ is high, the PFO model gave better prediction for the kinetics data than PSO models, contrary when the $C_0$ is low; the PSO model represents adequately the adsorption kinetic data.

At present, the more complex adsorption reaction models have been widely developed to describe the kinetics process of adsorption. Santosa developed the adsorption kinetics model that can interpret the equilibrium constant ($K$) and adsorption energy ($E$) from single set data [14]. The Santosa's model originated from assumption:

$$\frac{d\theta_A}{dt} = k_s(1-\theta_A)C_A - k_{ds}\theta_A \quad (7)$$

with the particular assumption $k_sC_0+k_{ds} \approx k_sC_0$, integrating Eq. (7) from 0 to $q_t$ and from 0 to $t$ for the $dt$, the linear expression was obtained:

$$\frac{1}{C_0 - Xq_e}\ln\left(\frac{q_e(C_0 - Xq_t)}{C_0(q_e - q_t)}\right) = k_s t \quad (8)$$

The Santosa's desorption rate constant ($k_d$) was obtained from the equation:

$$\ln\left(1 - \frac{q_t}{q_e}\right) = -\beta t \quad (9)$$

where, $\beta$ is equal to $k_sC_0 + k_{ds}$.

Later, Rusdiarso *et al.* [15] proposed a kinetics model which has similar significance with the Santosa's model. The Rusdiarso *et al.*'s model originated from the assumption [15–17]:

$$\frac{dx}{dt} = k_a(C_0 - x)(C_b - x) - k_d x \quad (10)$$

Taking integration of Eq. (10) from ($C_0C_b$) to ($C_0C_b-x_ex$), 0 to $x$, and 0 to $t$ results

$$\ln\left(\frac{C_0C_b - x_e x}{x_e - x}\right) = k_a\left(\frac{C_0C_b - x_e^2}{x_e}\right)t - \ln\left(\frac{x_e}{C_0C_b}\right) \quad (11)$$

Recently, the adsorption rate constant ($k_a$) in the kinetics models reported has not always been constant [18]. The uncertain $k_a$ value is also essential obstacle to the adsorption kinetics comparison among adsorbents. The $k_a$ is significantly affected by the initial reaction conditions, which one of them is the initial solute concentration ($C_0$) [19]. Although some researchers have been recognize this phenomenon there is limited further effort to address the problem [20–22]. To date, very limited study has evaluated the dependency of kinetics parameter with the $C_0$ of the various mentioned kinetics models.

In this study, the dependency of adsorption kinetics parameters obtained from various kinetics models of different adsorbent as the function $C_0$ was investigated. Those kinetics models have been examined to the widely applied adsorbent: humic acid (HA) [23]. Our previous study reported that the dry horse dung powder is promising as a source of HA-like adsorbent. In order to increase the stability and adsorption capacity, the horse dung humic acid functionalized chitin (HDHA-Ch) and horse dung humic acid functionalized magnetite (HDHA-$Fe_3O_4$) has been prepared in this work. The synthesized adsorbent was applied to Pb(II) and Ni(II) as solute for HDHA-Ch adsorbent, and Pb(II) and methylene blue (MB) as solute for HDHA-$Fe_3O_4$ adsorbent. Further, the comparison of characterization, adsorption capacity, and the optimum condition adsorption of as-prepared adsorbent were also investigated in this paper.

## 2. Materials and Methods

### 2.1 Materials

The HDHA was extracted from three month aged horse dung material in 30 cm depth from soil surfaces by the Stevenson's procedure [24]. Chitin was isolated from wasted shrimp shell of local seafood restaurant in Yogyakarta, Indonesia through No *et al.* methods [25]. All chemicals used in this work i.e. sodium hydroxide pellet, hydrochloric acid 37%, hydrofluoric acid 48%, ammonia solution 25%, iron(III) chloride hexahydrate, iron(II) sulphate heptahydrate, lead(II) acetate and nickel(II) acetate as source of metal ion, and the Methylene Blue (MB) dye as solute were analytical grade produced by Merck® without further purification.

### 2.2 Instrumentations

Functional group analysis was conducted by Fourier transform infra-red spectroscopy (FT-IR, Shimadzu Prestige 21). Surface morphology and elemental composition was analyzed by scanning electron microscopy-Energy dispersive X-ray (SEM-EDX, Phenom Desktop ProXL). Average size analysis of adsorbent was characterized by combination of transmission electron microscopy (TEM, JEOL JEM-1400) image with the Image-J free software. Metal ions and dyes quantification was performed by atomic absorption spectroscopy (AAS, Perkin Elmer 3110) and UV-Vis spectrophotometer (UV-1800 Shimadzu), respectively. Measurement of magnetic strength and pH in solution was conducted by Vibrating Sample Magnetometer (VSM, Oxford 1.2H) and pH meter HI98100 Hanna Instrument. Thermal stability was recorded by differential thermal analyzed (DTA, DTG-60 Shimadzu).

### 2.3 Preparation of Adsorbents

The HDHA-Ch was synthesized refer to methods published by Santosa *et al.* [26] through replacing peat HA with HDHA. Briefly, 40 g of chitin was stirred in 250 mL HCl 0.5 M for 24 h until the gelatinous chitin formed. The HDHA-Ch was prepared by reaction of 4 g HDHA in 500 mL NaOH 0.5 M with the gelatinous chitin under the stirring for 6 h and followed by aging for 24 h. This procedure should be yield HDHAC with the stability of the HDHA attached on chitin which have excellent stability at the widely range of pH.

The HDHA-$Fe_3O_4$ were prepared following procedure reported by Liu *et al.* [27] through dissolving 6.1 g $FeCl_3.6H_2O$ and 4.2 g $FeSO_4.7H_2O$ into 50 mL distilled water. The solution heated to 90 °C, then, two solution of 10 mL $NH_3$ 25% and the mixture of 0.5 g HDHA in 100 mL NaOH 0.1 M were simultaneously added. The mixture was stirred for 60 min and then aged for 24 h. The black sediments of HDHA-$Fe_3O_4$ was rinsed to neutral pH, and dried in a vacuum oven at 50 °C.

2.4 Effect of pH and Stability Study

The effect of pH on the adsorption of Pb(II) and MB onto HDHA-$Fe_3O_4$ and Pb(II) and Ni(II) onto HDHA-Ch over a pH range of 2–10 was investigated. A series of 25 mL solute in glass flasks at desired concentration (Pb(II) = Ni(II) = 50 mg/L; MB = 25 mg/L) with pH medium 2.0-8.0 range were prepared. Into each flask, 50 mg of the adsorbent was inserted and shake for 2 h. After the adsorbent was separated, the remaining metal ions and MB dyes in solutions was quantified with AAS and UV-Vis spectrophotometer, respectively. The amount of solute per unit weight of adsorbent was calculated by the following equation:

$$q_e = \frac{V(C_0 - C_e)}{W \times 1000} \quad (12)$$

The stability of HDHA-$Fe_3O_4$ and HDHA-Ch was analyzed in two aspects: pH and thermal stability. pH stability in solid form was evaluated at different medium pH. One hundred mg of HDHA-$Fe_3O_4$ and HDHA-Ch was exposed to solutions with medium pH ranging from 2.0 to 13.0. After stirring for 24 h, the solid was separated with an external magnet and weighed carefully. Thermal stability was evaluated by DTA instrument.

2.5 Determining of Adsorption Capacity and Energy

A series of 50 mL conical Pyrex glass flasks was filled with 25 mL solution of solute of desired concentration (20, 40, 60, 80, 100, 150, and 200 mg/L) and adjusted to the optimum pH at room temperature. Then, 50 g of adsorbent was added to each flask and kept in isothermal shaker (25 °C) at 200 rpm until equilibrium was reached. Preliminary test showed that after 180 min, the solutes concentration remain unchanged significantly. After this period, the solution was separated with the adsorbent and analyzed spectrophotometrically for the solute remained in the solution. The amount of solute per unit weight of adsorbent, $q$ (mg/g) was calculated by the Eq. (12).

2.6 The Study of Kinetics with the Dynamic $C_0$

The batch type reactor was employed to study the effect of contact time at the varied $C_0$. For this purpose, a number of 50 mL flasks containing 25 mL of desired solute concentration (Pb(II) = Ni(II) = 20, 50, 100, and 400 mg/L and MB = 10, 25, 50, and 100 mg/L) were agitated in thermostat shaker at 200 rpm. Fifty mg of adsorbents was added into each flask at room temperature, 298 K. The solution of each specified flask was separated from the adsorbents at different time interval (5, 10, 20, 30, 40, 60, 90, 120, and 180 min) and analyzed for the uptake of solute.

The kinetics data was applied to the Boyd and Webber-Morris (represent the adsorption diffusion model) and Lagergren, Ho, and recent

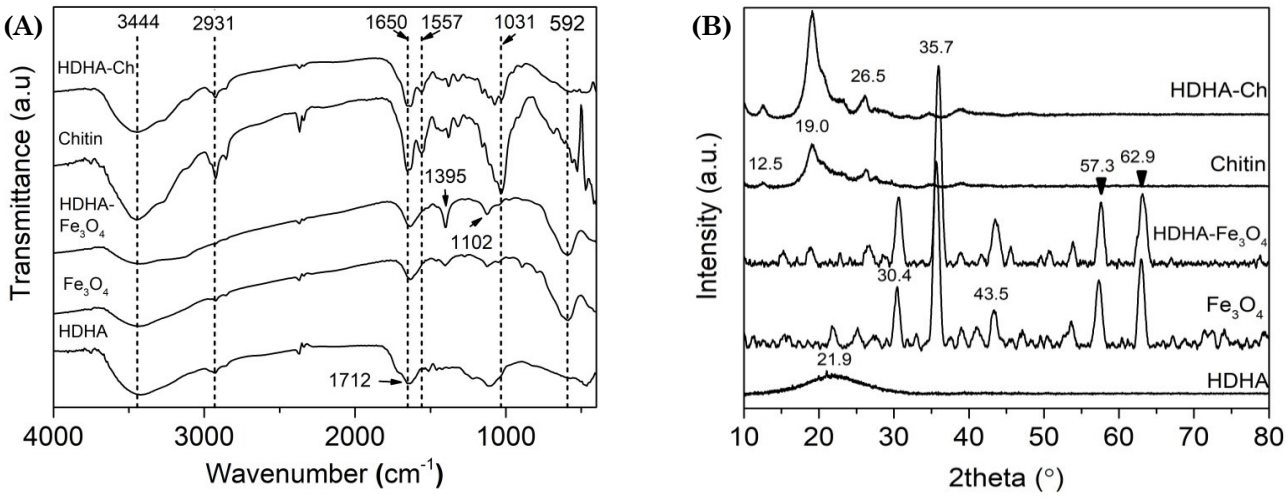


Figure 1. FT-IR spectra (A) and XRD diffractogram (B) of chitin, HDHA, $Fe_3O_4$, HDHA-Ch, and HDHA-$Fe_3O_4$.

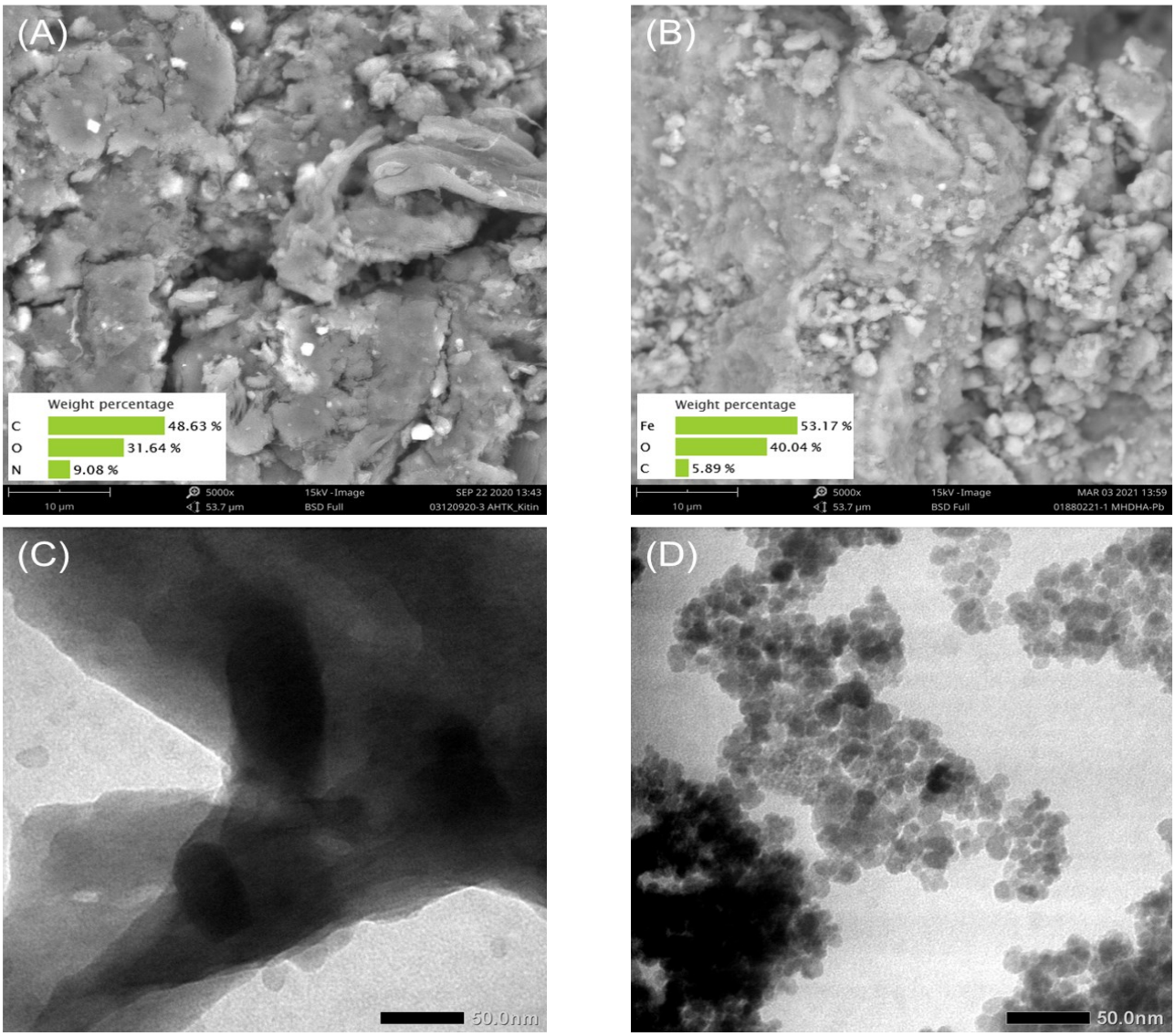


Figure 2. Surface morphology and composition of HDHA-Ch (A) and HDHA-$Fe_3O_4$ (B) by SEM-EDX; TEM image of HDHA-Ch (C) and HDHA-$Fe_3O_4$ (D).

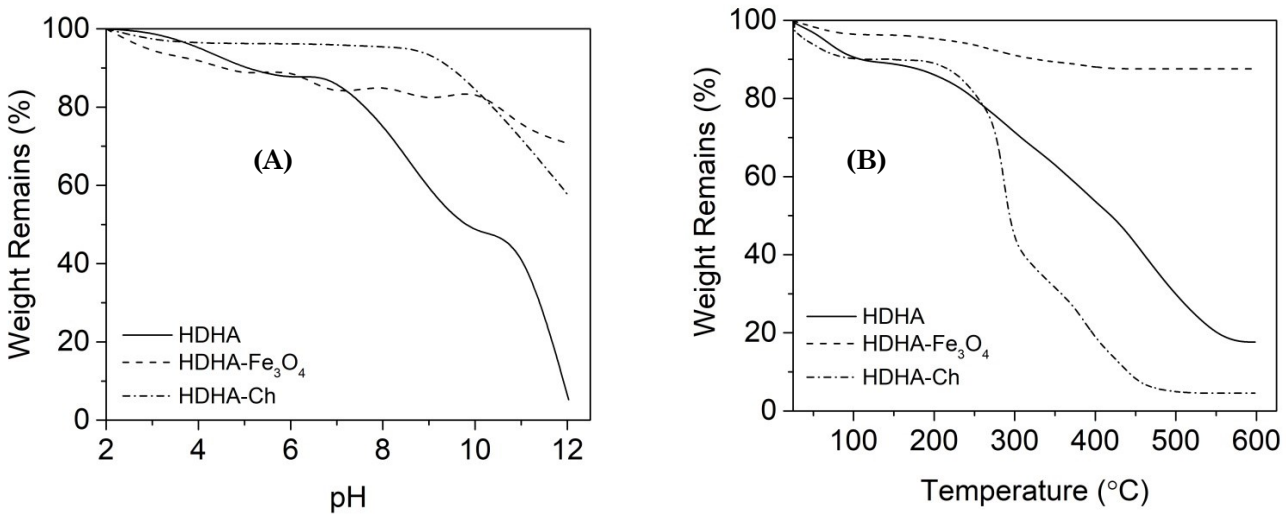


Figure 3. (A) stability comparison of HDHA-Ch, HDHA-$Fe_3O_4$, and HDHA in alkaline solution; (B) the TGA curves of the HDHA, HDHA-Ch, and HDHA-$Fe_3O_4$.

developed model: Santosa and RBS (represent the adsorption reaction model).

## 3. Results and Discussion

### 3.1 Characterization of Adsorbent

The extracted HDHA shows the humic-like substance since it exhibit five characteristic peaks of HA: 3444, 2931, 1721, 1650, and 1208 $cm^{-1}$ that represents the O−H stretching; aliphatic C−H stretching; C=O of COOH and ketones; aromatic C=C and strongly H-bonded C=O of conjugated ketones; and C−O stretching of COOH, respectively (Figure 1A) [24]. The peak at 1102 $cm^{-1}$ denotes the C−O stretching of unhumified polysaccharide substance or Si−O of silicate impurities. The successful isolated chitin presented in primary wavenumber at 3444, 2931, 1650, 1557 (N−H bending), and 1031 $cm^{-1}$ (C−N stretching) [25,28,29]. The Fe−O stretching vibration of synthesized $Fe_3O_4$ was identified at 592 $cm^{-1}$ [27,30]. Emerging peak at 1557 and 1031 $cm^{-1}$ in HDHA-Ch spectra and 592 $cm^{-1}$ at HDHA-$Fe_3O_4$ spectra (Figure 1A) indicates the successful incorporation of chitin and $Fe_3O_4$ into HDHA, respectively.

The XRD patterns of the isolated chitins and the HDHA-Ch showed an identical three sharp peaks at 12.5°, 19.0°, and 26.5° (Figure 1B), which exhibited successful modification HDHA with chitin. It is reported in the literature that these positions of the peaks indicate the chitin is in the α-form [31]. The identical characteristic peak of $Fe_3O_4$ with HDHA-$Fe_3O_4$ was shown in Figure 1B. The peaks at 30.4°, 35.7°, 43.5°, 57.3°, and 62.9°, which corresponding to (220), (311), (400), (511), and (411) reflections were suitable with the standard pattern of $Fe_3O_4$ spinel structure (JCPDS 19-0629) [44–45]. Unobserved crystal damage of HDHA-$Fe_3O_4$ indicated the successful incorporation of HDHA on $Fe_3O_4$. Further, the decreasing magnetic strength of $Fe_3O_4$ (80.25 emu/g) and HDHA-$Fe_3O_4$ (62.95 emu/g) sustained the successful of the HDHA-$Fe_3O_4$ synthesized process.

The surface morphologies of the HDHA-Ch and HDHA-$Fe_3O_4$ were investigated with SEM-EDX analysis and the results are shown in Figure 2(A-B). The SEM image of the HDHA-Ch (Figure 2A) reveals that the surface is smooth with stringy textures dominated by carbon (48.63%), oxygen (31.64%), and nitrogen (9.08%). The results of the TEM images also indicate identical textures (Figure 2C). While the HDHA-$Fe_3O_4$ has rougher morphology with a round shape structure dominated by iron (53.17%), oxygen (40.04%), and carbon (5.89%) (Figure 1B). The TEM image showed that the HDHA-$Fe_3O_4$ existed in non-uniform aggregates and round features with $Fe_3O_4$ core (Figure 2D). Size analysis using image-J software shows that the average diameter of HDHA-$Fe_3O_4$ is 15 nm. Similarly, previous report by Illés and Tombácz revealed that $Fe_3O_4$ nanoparticles have ~10 nm primary size of round to non-uniform fractal aggregates [34].

The stability of HDHA-Ch and HDHA-$Fe_3O_4$ compared with HDHA in alkaline solution are shown in Figure 3A. At pH 5.0, the HDHA show 10% of weight loss due to the starting of carboxylic and phenolic group deprotonation. At pH higher than 7, weight loss was extremely occurred and only less than 5% of the weight of HDHA remained when pH reached 12. After incorporation with chitin, the stability of HDHA-Ch was improved to pH 9, and only lost 47% of the HDHA-Ch weight (Figure 3A). Previous report by Santosa *et al.* [28] demonstrated the correspond results. Similarly, HDHA-$Fe_3O_4$ show the improved stability until pH 10 with the 83% remained weight. The stability improvement of HA or HA-like substance by $Fe_3O_4$ incorporation has been widely reported [23,27,35–37]. The results indicate that modification of HDHA with the chitin and $Fe_3O_4$ has improved the stability in alkaline solution.

The TGA curves for the HDHA, HDHA-Ch, and HDHA-$Fe_3O_4$ are shown in Figure 3B. All of the materials show mass loss approximately 5-10% up to 100 °C, which attributed to evaporation of water from the sample. Above 150 °C, the thermal stability of HDHA gradually decreased and completes at 570 °C. The HDHA-Ch thermal profile was quite un-degraded after water evaporation up to 260 °C. However, HDHA-Ch starts to descend quickly at 267 °C and completes its degradation at 460 °C. Compare with the HDHA and HDHA-Ch, the TGA result of HDHA-$Fe_3O_4$ shown significant stability above 90% un-degraded when the temperature heating up to 570 °C.

### 3.2 Effect of pH

pH is an essential factor which affected the affinity of binding solute onto the adsorbent. The sorbent's surface charge as well as the structure of the solute speciation is highly influenced by pH. At low pH (high amount of $H^+$) adsorption of the metal ion and the MB was quietly low (Figure 4). In literature, the low adsorption of metals ion observed in low pH has been attributed to several factors: repulsion be-

tween adsorbent positively charge surfaces and the metal cations, competition between $H^+$ and free metal cations to adsorbed on to adsorbent active sites, protonation of surface functional group lead to lower formation of complexes with metal ions, and combination of these factors [20].

In this study, the highest adsorbed metal ion and MB was achieved at pH optimum ~5 and ~6, respectively. At this condition, deprotonation was occurred and the solid adsorbent's surface became negatively charged. As a result, electrostatic repulsion decreased and it enhanced the positively charged metal ions and MB adsorption. At higher pH than pH optimum, the adsorbed metal ion was sharply decreased due to the formation of solid metal hydroxide [38]. For MB, the decreasing adsorbed MB was might be caused by competition between the $OH^-$ ions and the negatively charged surface of the adsorbents [39]. Similar trend was reported in the adsorption one of Pb(II), Ni(II), and MB on HA-chitin [28], peat HA [40], magnetic/HA/chitosan [41], magnetite-humin [42], and magnetite-HA [43].

### 3.3 Adsorption Capacity and Energy

In order to deliver the design of the adsorption system, it is important to establish the most appropriate correlation for the equilibrium curves. In this study four linearized adsorption isotherm models: the Langmuir, Freundlich, Temkin, and Dubinin-Radushkevich (D-R) were applied to fit the equilibrium data of adsorbed Pb(II)/Ni(II) onto HDHA-Ch and Pb(II)/MB onto HDHA $Fe_3O_4$ (Figure S1).

Langmuir isotherm assumes the monolayer adsorption on the finite and uniform active sites with no interaction among solute in the plane of surface [44]. The linear form of Langmuir isotherm equation is gives as:

$$\frac{C_e}{q_e} = \frac{1}{bK_L} + \frac{1}{b}C_e \quad (13)$$

where $C_e$ (mol/L) is the equilibrium concentration of the solute, $q_e$ (mol/g or mg/g) is amount of solute adsorbed per unit mass adsorbent, $b$ (mg/g or mol/g) and $K_L$ (L/mol) are Langmuir adsorption capacity and equilibrium constant, respectively.

The important features of the Langmuir model can be expressed in terms of dimensionless constant called separation factor of equilibrium parameter, $R_L$ described by Weber and Cakkravorti [45]:

$$R_L = \frac{1}{1 + K_L C_0} \quad (14)$$

which the $R_L$ values indicated to irreversible ($R_L$=0), favorable (0<$R_L$<1), and unfavorable ($R_L$>1).

Figure 5 showed the calculated $R_L$ values vs. the initial solute concentration ($C_0$). All the RL values were between 0 and 1, indicated the adsorption of solute: Pb(II)/MB and Pb(II)/Ni(II) anto HDHA-$Fe_3O_4$ and HDHA-Ch was favorable at the condition being studied, respectively. However, the $R_L$ values decreased as the $C_0$ increased from 20 to 200 mg/L, indicated that the adsorption was more favorable at higher $C_0$.

Freundlich model is an experimental equation based on heterogeneous surface sites [46]. It is assumed that the stronger sites are occupied first and that the binding strength decrease with the increasing degree of occupation. The linear form of Freundlich model is

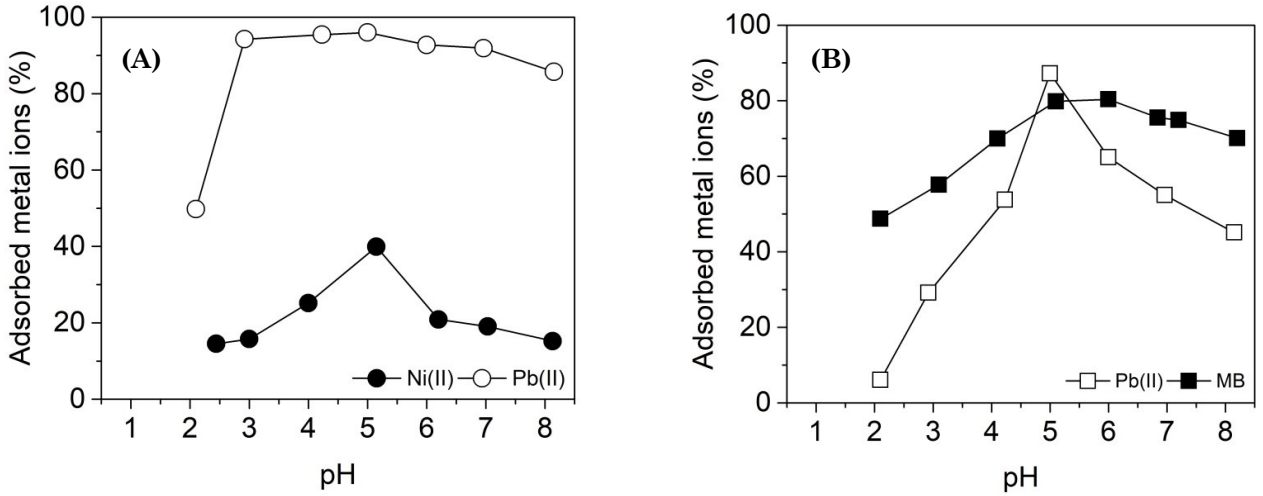


Figure 4. Effect of the pH on the adsorbed Pb(II) and Ni(II) onto HDHA-Ch (A) and Pb(II) and MB onto HDHA-$Fe_3O_4$.

given by:

$$\ln q_e = \ln B + \frac{1}{n}\ln C_e \quad (15)$$

where B is the multilayer adsorption capacity (mg/g (L/mg)$^{1/n}$) that represents the quantity of the solute adsorbed onto the adsorbent for a unit equilibrium concentration. $n$ is the Freundlich constant that indicates how favorable the adsorption process. The slope of $1/n$ value ranging between 0 and 1 measures the surface heterogeneity, becoming more heterogeneous when its value gets closer to zero. The value of $1/n$ < 1 indicates a normal Langmuir and $1/n$ > 1 indicates of cooperative adsorption.

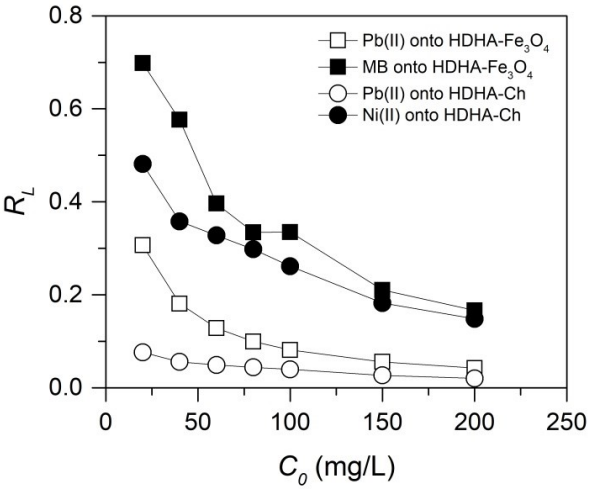


Figure 5. Effect of initial solute concentration ($C_0$) on separation factor ($R_L$).

Temkin isotherm [47] explains the solute-adsorbent interaction based on the assumption that there is an indirect relationship between sorption energy and their interaction. Temkin isotherm is expressed as:

$$q_e = \frac{RT}{b_T}\ln A_T + \frac{RT}{b_T}\ln C_e \quad (16)$$

where $b_T$ (J/mol) relates to the heat of adsorption, which it decrease linearly with coverage due to solute-adsorbent interaction. $A_T$ (L/g) is the equilibrium binding constant corresponding to the maximum binding energy. R (8.314 J/mol K) and T (K) are universal gas constant and absolute temperature, respectively.

D-R isotherm is defined by:

$$\ln q_e = \ln q_{DR} - B_{DR}\varepsilon^2 \quad (17)$$

where, $\varepsilon$ correlates as Polanyi potential, $\varepsilon$ = RT ln [1+(1/$C_e$)]. $B_{DR}$ gives the mean free energy ($E_{DR}$) of sorption per molecule of solute when it transferred to the surface of the adsorbent from infinity in the solution [7]. $E_{DR}$ can be computed using the relationship:

$$E_{DR} = \frac{1}{\sqrt{2B_{DR}}} \quad (18)$$

and it believed to determine the interaction of the solute and the adsorbent: 0<$E_{DR}$<7 kJ/mol indicates the physical interaction, and 8<$E_{DR}$ <16 indicates adsorption comprised with the ion exchange between solute and adsorbent [2,48].

Table 1. Correlation coefficient ($R^2$) and corresponding parameters of four isotherm model of Pb(II)/MB and Pb(II)/Ni(II) onto HDHA-$Fe_3O_4$ and HDHA-Ch, respectively.

| Isotherm Model | Parameters | Solute-Adsorbent | | | |
|---|---|---|---|---|---|
| | | Pb(II) onto HDHA-$Fe_3O_4$ | MB onto HDHA-$Fe_3O_4$ | Pb(II) onto HDHA-Ch | Ni(II) onto HDHA-Ch |
| Langmuir | $b$ (×10$^{-5}$ mol/g) | 27.52 | 9.77 | 58.87 | 97.57 |
| | $b$ (mg/g) | 57.02 | 31.25 | 121.96 | 57.26 |
| | $K_L$ (L/mol) | 23443.87 | 6542.25 | 50112.09 | 1719.05 |
| | $E_L$ (kJ/mol) | 25.10 | 21.91 | 26.81 | 18.46 |
| | $R^2$ | 0.9985 | 0.9923 | 0.9940 | 0.9969 |
| Freundlich | $B$ (×10$^{-5}$ mol/g) | 225.07 | 22.51 | 185.09 | 726.85 |
| | $B$ (mg/g) | 465.90 | 72.0 | 592.00 | 2324.84 |
| | $1/n$ | 0.31 | 0.19 | 0.15 | 0.35 |
| | $R^2$ | 0.9737 | 0.9557 | 0.8829 | 0.9834 |
| Temkin | $b_T$ (J/mol) | 393.32 | 268.84 | 183.84 | 200.92 |
| | $A_T$ (L/g) | 4.50 | 0.15 | 62.32 | 3.34 |
| | $R^2$ | 0.9813 | 0.9964 | 0.8902 | 0.9918 |
| D-R | $q_D$ (×10$^{-4}$ mol/g) | 7.03 | 2.97 | 9.12 | 5.59 |
| | $q_D$ (mg/g) | 145.69 | 95.03 | 298.93 | 178.71 |
| | $B_{DR}$ (×10$^{-9}$ mol$^2$/J$^2$) | 2.99 | 3.84 | 1.29 | 1.69 |
| | $E_{DR}$ (kJ/mol) | 12.91 | 11.18 | 19.69 | 17.21 |
| | $R^2$ | 0.9902 | 0.9818 | 0.8896 | 0.9923 |

All the correlation coefficient ($R^2$) values and the corresponding parameters from four isotherm models applied for adsorption of Pb(II)/MB onto HDHA-$Fe_3O_4$ and Pb(II)/Ni(II) onto HDHA-Ch are summarized in Table 1. The Langmuir model gave the highest $R^2$ values which were greater than 0.96 (satisfactory) of all experiment, showing that the adsorption of the solute onto the adsorbent in this work was best described by this model. The results agreed with the works carried out by many previous researchers which reported that the Langmuir model gave a better fit than the other isotherm model on the adsorption of HA-based modified adsorbents (Table 2).

The highest monolayer adsorption capacity ($b$) was achieved by the adsorption of Ni(II) onto HDHA-Ch ($97.57\times10^{-5}$ mol/g). In general, HDHA-Ch shows the higher monolayer adsorption capacity than HDHA-$Fe_3O_4$. Nevertheless, HDHA-Ch still required an additional step (filtering/centrifugation) in the separation of post-adsorption adsorbents, while HDHA-$Fe_3O_4$ demonstrated easy and quick separation with an external magnet. Table 2 lists comparison the monolayer adsorption capacity of various HA-based modified adsorbents. The HDHA-$Fe_3O_4$ and HDHA-Ch prepared in this work showed relatively high adsorption capacity as compared to some previous works reported in the literature.

The value of $E_{DR}$ found in this work were 12.91 (Pb(II)) and 11.18 (MB) kJ/mol for HDHA-$Fe_3O_4$ adsorbent (Table 1), which implied ion exchange was the main mechanism involved in the adsorption process for this adsorbent. However, the value of $E_{DR}$ for HDHA-Ch adsorbent were 19.69 (Pb(II)) and 17.21(Ni(II)) kJ/mol, which implied a stronger chemical adsorption than ion exchange occurred for this adsorbents [49]. Further, the values of $b_T$ obtained from the Temkin isotherm ranging from 0.2 to 0.4 kJ/mol (Table 1) indicated that the adsorption energy of outer layer adsorbed solute in this work occurred via ion exchange mechanisms [50,51].

### 3.4 The Dependency of Kinetic Parameters as a Function of Initial Solute Concentration

The kinetics adsorption describes the rate of the solutes uptake on the adsorbent which controlled by the equilibrium reaction. The kinetics of solutes uptake is required for selecting optimum operating condition for large-scale batch process. The kinetics parameter, which is helpful for the prediction adsorption rate, gives important information for designing and modeling process. Thus, the dependency of the kinetics parameters was analyzed from the kinetic point of view.

Table 2. Comparison of monolayer adsorption capacity of Pb(II), MB, and Ni(II) solute onto various HA-modified adsorbents.

| Adsorbent | $R^2$ | Solute | $b$ (mg/g) | Particular condition | Ref. |
|---|---|---|---|---|---|
| HA-CMC/PMH | 0.9995 | MB | 666.67 | pH=~7; T=298 K | [70] |
| HA-$Fe_3O_4$ NPs | 0.9900 | MB | 200.00 | pH=10; T=298 K | [42] |
| HA-$Fe_3O_4$ | 0.9987 | MB | 108.81 | pH=11; T=298 K | [71] |
| HA/Perlite | 0.9662 | MB | 82.80 | pH=10; T=303 K | [72] |
| Peat Humin | 0.9980 | MB | 70.55 | pH=6.2; T=298 K | [43] |
| HDHA-$Fe_3O_4$ | 0.9923 | MB | 31.25 | pH=6; T=298 K | This work |
| Biopolymer HA | 0.9500 | MB | 20.83 | pH=7; T=298 K | [73] |
| River humus HA | 0.9625 | MB | 15.82 | pH=8; T=298 K | [74] |
| HDHA-Ch | 0.9940 | Pb(II) | 121.96 | pH=5.2; T=298 K | This work |
| $Fe_3O_4$/HA | 0.9900 | Pb(II) | 92.40 | pH=5.0; T=298 K | [27] |
| HA peat (Polland) | 0.9920 | Pb(II) | 82.31 | pH=5.0; T=298 K | [75] |
| Starch-HA | 0.9900 | Pb(II) | 58.82 | pH=5; T=298 K | [76] |
| HDHA-$Fe_3O_4$ | 0.9940 | Pb(II) | 57.02 | pH=5; T=298 K | This work |
| HA soil (India) | 0.8200 | Pb(II) | 19.16 | pH=5; T=298 K | [77] |
| HA Peat | 0.9960 | Pb(II) | 14.97 | pH=5.5; T=298 K | [40] |
| HA peat (Polland) | 0.9910 | Ni(II) | 61.27 | pH=5; T=298 K | [75] |
| HDHA-Ch | 0.9969 | Ni(II) | 57.26 | pH=5; T=298 K | This work |
| HA-Cellulose | 0.9600 | Ni(II) | 12.41 | pH=5; T=298 K | [78] |
| HA-Chitin | 0.9840 | Ni(II) | 5.86 | pH=8; T=298 | [28] |

The effect of different initial solute concentration ($C_0$) as function of time to the adsorbed solute at time $t$ ($q_t$) is shown in Figure 6. Adsorption of all solutes on the adsorbent showed the similar pattern. The rapid adsorption was occurred at first 10 min for all experiments that indicated an abundant of accessibly available active sites on the adsorbent surface [52]. At this stage, more than 70% of the adsorbent sites were saturated by the solutes. Thereafter, the adsorption rate slows dramatically as the active sites were progressively occupied by the solute molecule. Generally, the equilibrium has been reached after ~180 min; however the data shows that the equilibrium attains faster at the lower $C_0$. It was also observed that as the $C_0$ increases up to 400 mg/g, the adsorbed solute at equilibrium ($q_e$) increases but never surpass the monolayer adsorption capacity ($b$) of the particular system. Similar phenomenon was observed for the adsorption of MB onto activated carbon where the equilibrium time and adsorbed solute ($q_e$) was found to be increased when the initial MB concentration increased [53]. This observation could be explained by the chemodynamics theory that in the process of solute adsorption, initially the solute molecules have to first encounter the outer boundary layer and then diffuse from the boundary layer film onto adsorbent surface and then finally, they have to diffuse into the porous structure of the adsorbent [54,55]. Therefore, the higher initial solute concentrations ($C_0$) will take relatively longer contact time to attain equilibrium due to higher amount of dye molecules, also, when the initial solute concentration increased ($C_0$), the mass transfer driving force would become larger, hence resulting in higher adsorption of solute [53].

The mechanism involved in this adsorption system, investigated by adsorption reaction model: Lagergren (Eq. 3), Ho (Eq. 6), Santosa (Eq. 8), and RBS (Eq. 11) and adsorption diffusion model: Boyd (Eq. 1) and Weber-Morris (Eq. 2). The plot of the kinetics data to the linearized adsorption reaction models has been presented in Figure S2-S5 and the corresponding kinetic parameters were listed in Table S1.

As can be seen, the relatively higher value of the correlation coefficient ($R^2$), which is an essential precedent in the determination of proper fit, for the Ho model compared to those of the Lagergren, Santosa, and RBS models as well as the very close similarity of the experi-

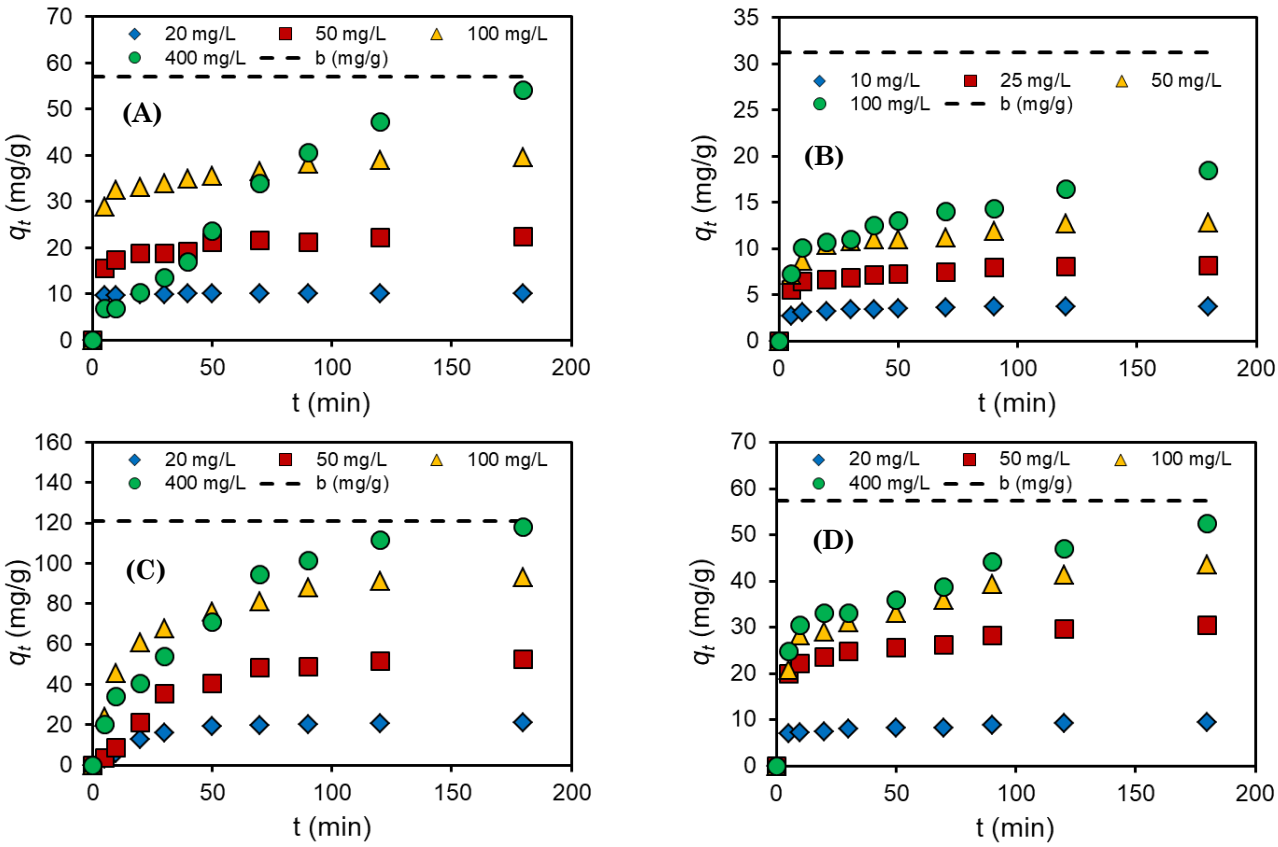


Figure 6. The effect of initial solute concentration ($C_0$) as function of time to the adsorbed (A) Pb(II) onto HDHA-$Fe_3O_4$, (B) MB onto HDHA-$Fe_3O_4$, (C) Pb(II) onto HDHA-Ch, and (D) Ni(II) onto HDHA-Ch at time $t$ ($q_t$).

mental and calculation of adsorbed solute at equilibrium ($q_e$) values indicates that the adsorption mechanism is best described by the Ho model, except for the Pb(II) adsorption onto HDHA-Ch. However, it was observed that for the adsorption of Pb(II)/MB onto HDHA-$Fe_3O_4$ and Ni(II) onto HDHA-Ch, the Ho's correlation coefficient ($R^2$) is closer to unity at the low initial solute concentration ($C_0$) and tend to decrease with the increasing of initial solute concentration (Figure 7A). This result was in line with the report in literature.

Previously, Sabarinathan *et al*. [56] reported that the $R^2$ value of Ho model of the MB adsorption onto polyoxometalate decreased from 0.8979 to 0.5905 with the increase of $C_0$ from 140 to 300 mg/L. Almeida *et al*. [57] reported the decreasing of Ho's $R^2$ value in MB adsorption on montmorillonite clay from 1.0000 to 0.9951 when the $C_0$ varied from 200 to 1000 mg/L. The best fit Ho model to the adsorption system at low $C_0$ in literature was shown in research of resorcinol onto CTAB/NaOH/flyash [58], MB onto BBLS-CA [59], Cu(II) onto dried algal [60], benzene and toluene onto coconut shell-based AC [61], methyl orange onto NiO and CuO NPs [62], and dyes onto peat [9]. Further, Zhang [3] and Marczewski [63] found that the best condition for the Ho model was at the equilibrium surface coverage ($\theta$) approach to 1. Guo and Wang found that three conditions could represent the best-fitted the Ho model: the low $C_0$, at the final stage of the adsorption process, and the adsorbent has abundant active sites [65].

Meanwhile, the Lagergren $R^2$ trend was closer to unity with the increasing of $C_0$. Contrary, when the Lagergren's $R^2$ is the best fit to the adsorption system at low $C_0$ (in Pb(II) adsorption onto HDHA-Ch case), the Ho's $R^2$ tend to increase at high $C_0$ (Figure 7B). The previous study reported that the Lagergren model fits well only for the rapid initial phase that occurs for a contact time of 0–10 min [66–68]. The initial rapid adsorption (in the first 10 min) is strongly suspected as a chemisorption process. Thereafter, for the second phase, the profile suggests a physisorption mechanism, which is possibly governed by a diffusion mechanism [52]. The study confirms that the Lagergren model is not appropriate to predict the adsorption kinetics for the entire adsorption period due to the changing adsorption mechanisms at the initial and second phase. Considering the fact to this work, the decreasing Ho's $R^2$ at the high $C_0$ is strongly considered by the changing adsorption mechanism. This revealed that adsorption mechanism changes not only due to contact time but also due to changes because $C_0$.

The dependency of the kinetics rates to the $C_0$ was presented in Figure 8. It can be seen that rate constant ($k$) of all the kinetics models, including the Ho kinetics constant ($k_{Ho}$) which was appropriate to this work, decreased with the increased $C_0$. This observation can be explained by the fact that the adsorption process takes a longer time to reach equilibrium at higher $C_0$. Although the adsorbed solute at equilibrium ($q_e$) is higher at high $C_0$ than at low $C_0$, the amount of adsorbed solute adsorbed per unit of time is less, this causes the rate constant to decrease as the $C_0$ increases. The decreasing adsorption rate constant ($k_a$) was accompanied by the decreasing desorption rate constant ($k_d$) which was estimated by the Santosa and RBS kinetic model (Table S1). It can be seen in the Table S1 that the Santosa kinetic model is possible to estimate $k_d$ when the $C_0$ is high, while the RBS kinetic model is possible at all $C_0$ values. Previous studies of the adsorption of Cu(II) on RSAC (rubber wood sawdust-activated carbon) [68], 2,4,6-trichlorophenol (TCP) on activated carbon prepared from oil palm empty fruit bunch [7], Cu(II) and Zn(II) on HA [69], and MB on montmorillonite clay [57] showed similar result in the decreasing of $k_{Ho}$ value at the higher $C_0$.

### 3.5 Adsorption Mechanism by Adsorption Diffusion Model

The diffusion mechanism was identified by the intraparticle diffusion model based on the theory of Weber and Morris [6]. It is an empirically found that the uptake of solute varies almost proportionally with $t^{1/2}$ rather than with the contact time $t$. According to the Equation (2) the $C_i$ intercept of stages $i$, give an idea about the thickness of boundary layer, the larger the $C_i$, the greater the boundary layer effect. If intraparticle diffusion plot gives straight line and passes through the origin, the rate limiting adsorption process is only due to the intraparticle diffusion. Otherwise, some other mechanism along with intraparticle diffusion is involved.

For intraparticle diffusion plots, the first, sharper region is the external surface adsorption or instantaneous adsorption [7]. The second region indicates when the intraparticle diffusion starts to slow down due to the low solute concentrations left in the solutions at the final equilibrium stage. Referring to Figure 9, for all $C_0$, the first stage was completed within the first 10 min and the second stage of intraparti-

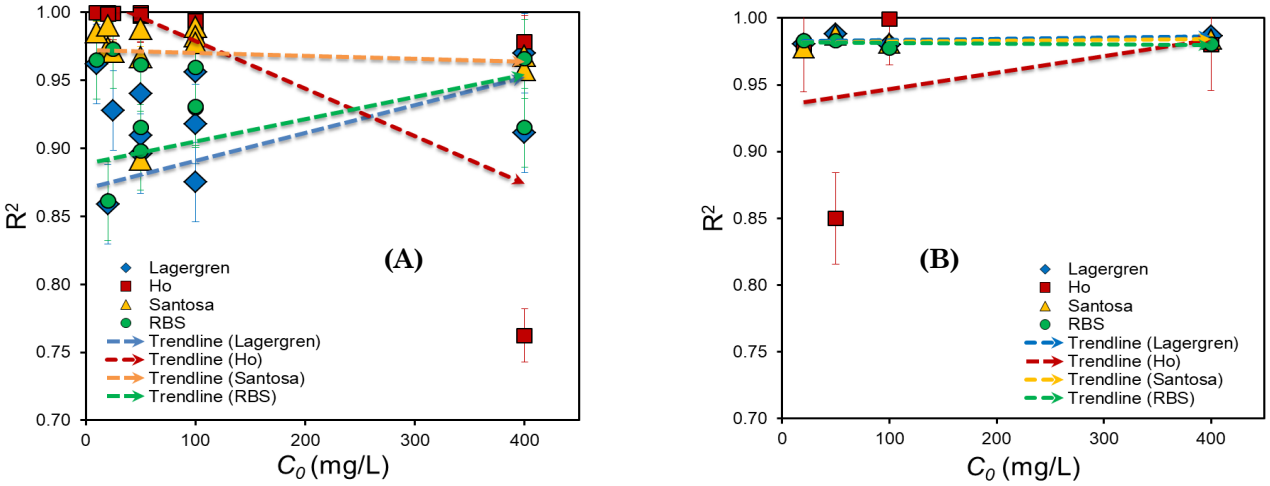


Figure 7. The effect of initial solute concentration ($C_0$) to the observed kinetics model's correlation coefficient ($R^2$) of the adsorption of (A) Pb(II)/MB onto HDHA-$Fe_3O_4$ and Ni(II) onto HDHA-Ch and (B) Pb(II) onto HDHA-Ch.

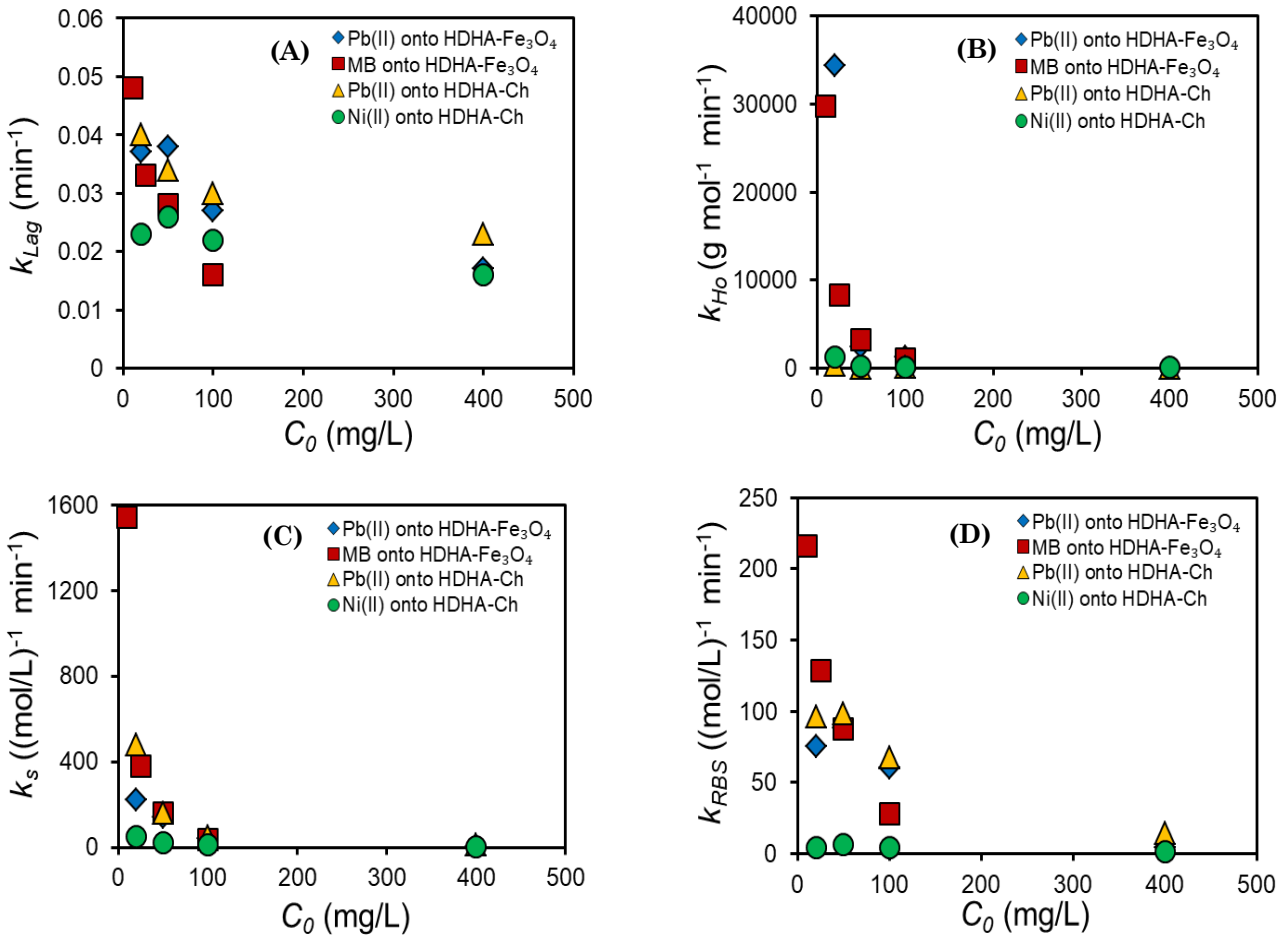


Figure 8. The dependency of the kinetics rates constant ($k$) obtained from (A) Lagergren, (B) Ho, (C) Santosa, and (D) RBS kinetics model to the initial solute concentration ($C_0$).

cle diffusion limiting control was then attained at the higher $C_0$, due to the proximity of linear adsorption to intersect the origin. The different stages of adsorbed solute indicated that the adsorption rate was initially faster and then slowed down with the increasing of time.

It was shown in Figure 9 that intraparticle diffusion is the rate limiting at first stage. At second stage, the linear lines did not intersect the origin indicated that intraparticle diffusion was not the only rate limiting mechanism in the adsorption process. This deviation from the origin or near saturation might be due to the difference in the mass transfer rate in the first and second stages of adsorption [69]. It was also observed that at higher $C_0$, the deviation becomes smaller and lead to the intersection with the origin. This can be explained by changes in adsorption mechanisms when the initial solute concentration ($C_0$) changes. The values of $k_{IP\text{-}i}$, $C_i$, and correlation coefficient ($R^2$) obtained from the plots are given in Table 3. The $k_{IP\text{-}i}$ values were found to be generally increased with the increasing $C_0$ which was due to the greater driving force [7].

In order to predict the actual slow step involved in the adsorption process, the kinetic data were analyzed using the Boyd model given by Eq. (1). The calculated $B_t$ values plotted against time, $t$ (min) was shown in Figure 10. The linear lines for Pb(II) adsorption onto HDHA-$Fe_3O_4$ at $C_0$ = 20, 50, and 100 mg/L (Figure 10A) did not pass through the origin. This indicated that the adsorption was mainly driven by external mass transport where particle diffusion was the rate limiting step. Otherwise, the other linear lines were closely lead to intersect the origin (Figure 10A 400 mg/L, Figure 10B-D) which indicate the intraparticle diffusion is the rate limiting step [53].

## 4. Conclusions

This study evidently showed the dependency of the initial solute concentration ($C_0$) to the kinetics parameter value. The evaluation was conducted by humic-like (humic acid from dry horse dung powder, HDHA) modified adsorbent: HDHA-$Fe_3O_4$ and HDHA-Ch and Pb(II), MB, and Ni(II) as solute. The success synthesize of these adsorbents was characterized by FT-IR, SEM-EDX, TEM, VSM, and DTA. Under optimum condition, the adsorption of solute to the adsorbents was fitted well to the Langmuir monolayer isotherm model with the ad-

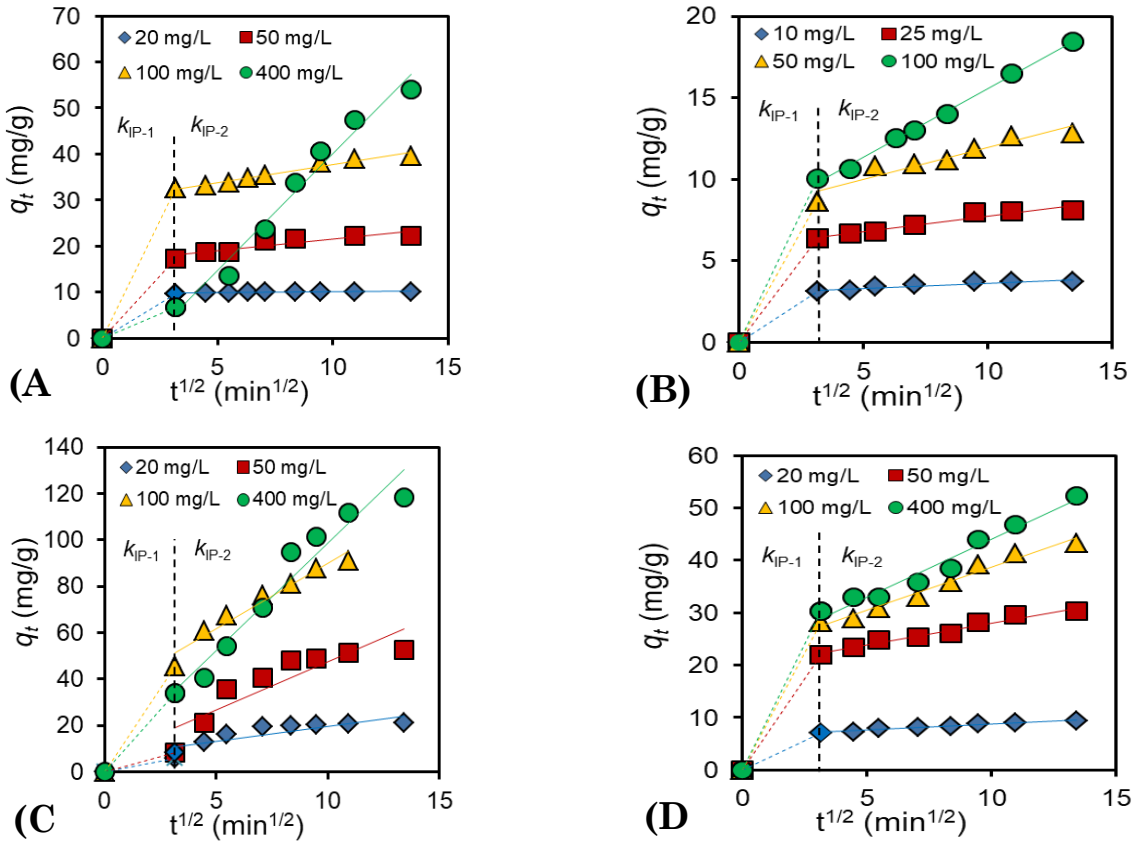


Figure 9. Plot of intraparticle diffusion model for adsorption of (A) Pb(II) onto HDHA $Fe_3O_4$, (B) MB onto HDHA-$Fe_3O_4$, (C) Pb(II)onto HDHA-Ch, and (D) Ni(II) onto HDHA-Ch.

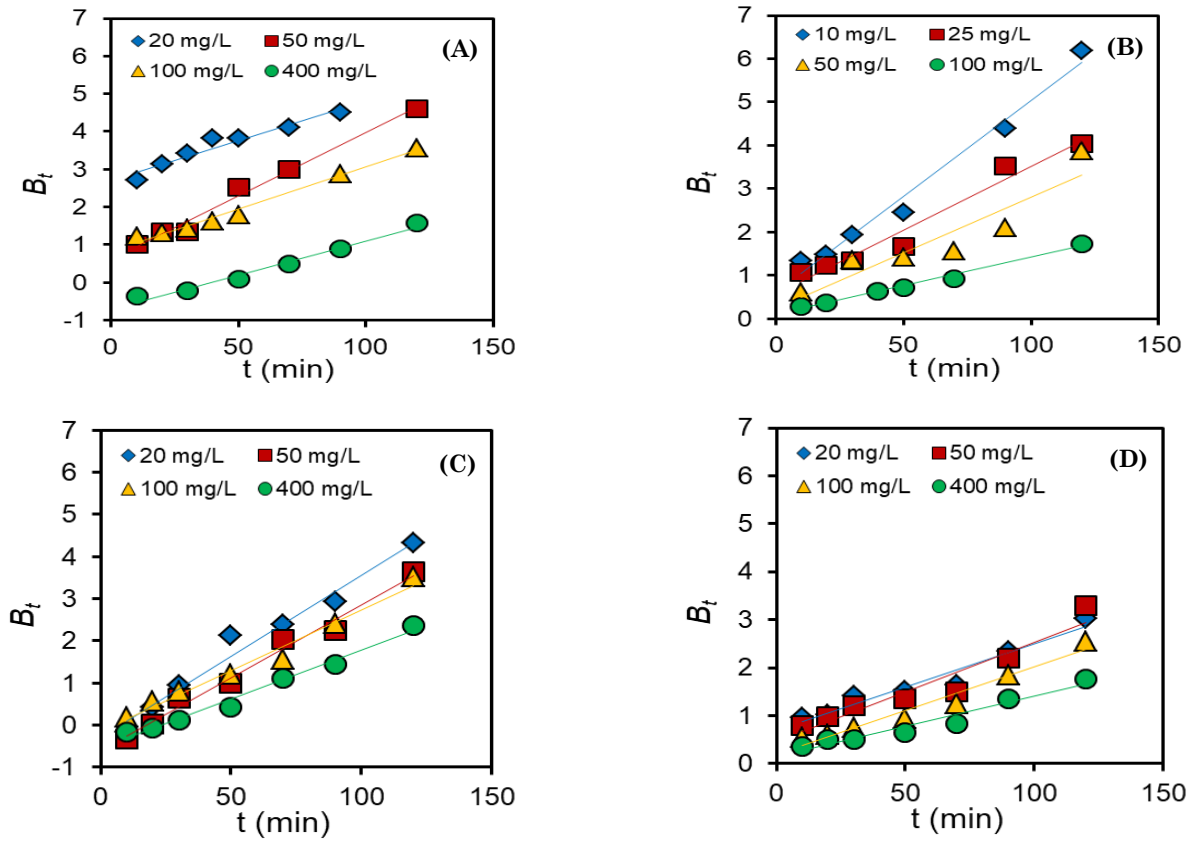


Figure 10. Boyd plot for adsorption of (A) Pb(II) onto HDHA $Fe_3O_4$, (B) MB onto HDHA-$Fe_3O_4$, (C) Pb(II)onto HDHA-Ch, and (D) Ni(II) onto HDHA-Ch.

Table 3. Intraparticle diffusion model constants and correlation coefficients for adsorption of Pb(II)/MB onto HDHA $Fe_3O_4$ and Pb(II)/Ni(II) onto HDHA-Ch.

| Solute | $C_0$ (mg/L) | $k_{IP-1}$ (mg/g min$^{1/2}$) | $k_{IP-2}$ (mg/g min$^{1/2}$) | $C_1$ | $C_2$ | $(R_1)^2$ | $(R_2)^2$ |
|---|---|---|---|---|---|---|---|
| Pb(II) onto HDHA-$Fe_3O_4$ | 20 | 2.14 | 0.04 | 0 | 9.68 | 1.0000 | 0.8577 |
| | 50 | 3.07 | 0.50 | 0 | 16.56 | 1.0000 | 0.8328 |
| | 100 | 5.47 | 0.78 | 0 | 29.92 | 1.0000 | 0.9645 |
| | 400 | 10.26 | 5.05 | 0 | 10.39 | 1.0000 | 0.9741 |
| MB onto HDHA-$Fe_3O_4$ | 10 | 0.99 | 0.06 | 0 | 3.00 | 1.0000 | 0.8764 |
| | 25 | 2.02 | 0.19 | 0 | 5.86 | 1.0000 | 0.9355 |
| | 50 | 2.72 | 0.40 | 0 | 8.00 | 1.0000 | 0.9000 |
| | 100 | 3.17 | 0.84 | 0 | 7.11 | 1.0000 | 0.9972 |
| Pb(II) onto HDHA-Ch | 20 | 1.87 | 1.29 | 0 | 6.90 | 1.0000 | 0.7058 |
| | 50 | 2.67 | 4.15 | 0 | 5.97 | 1.0000 | 0.8018 |
| | 100 | 14.42 | 5.61 | 0 | 33.62 | 1.0000 | 0.9540 |
| | 400 | 10.68 | 9.27 | 0 | 5.82 | 1.0000 | 0.9474 |
| Ni(II) onto HDHA-Ch | 20 | 2.26 | 0.23 | 0 | 6.49 | 1.0000 | 0.9556 |
| | 50 | 6.95 | 0.83 | 0 | 19.68 | 1.0000 | 0.9675 |
| | 100 | 8.91 | 1.64 | 0 | 21.92 | 1.0000 | 0.9750 |
| | 400 | 9.56 | 2.21 | 0 | 22.04 | 1.0000 | 0.9685 |

sorption capacity ($b$) of 57.02 mg/g for Pb(II) onto HDHA-$Fe_3O_4$, 31.25 mg/g for MB onto HDHA-$Fe_3O_{-4}$, 121.96 for Pb(II) onto HDHA-Ch, and 57.26 mg/g for Ni(II) onto HDHA-Ch. The value of adsorption energy by Dubinin-Radushkevich model ($E_{DR}$) indicate that ion exchange was the main mechanism for adsorption of Pb(II) (12.91 kJ/mol) and MB (11.18 kJ/mol) onto HDHA-$Fe_3O_4$ and a stronger chemical adsorption than ion exchange occurred for the adsorption of Pb(II) (19.69 kJ/mol) and MB (17.21 kJ/mol) onto HDHA-Ch. In this study, it was evidently proved that there is a change in the kinetics parameter value due to changes in the adsorption mechanism as an effect of dynamic $C_0$. It was observed that at higher $C_0$ the adsorbed solute at equilibrium ($q_e$) increases and it takes longer time to reach equilibrium. As a result, the kinetics rate constant ($k$) calculated from adsorption reaction model (Lagergren, Ho, Santosa, and RBS) was decreased. In general, Ho model exhibit higher correlation coefficient value ($R^2$) among other model at low $C_0$. At high $C_0$, Ho's $R^2$ tend to decrease while the Lagergren and RBS's $R^2$ was increased. The amendment mechanism from external mass transport to intra-particle diffusion as a rate limiting step was evidenced by Boyd and Weber-Morris kinetics model. Therefore, the outcomes of this study will contribute to the effective design and optimization of removal pollutant (dye and heavy metal) in wastewater by adsorption equipment.

## Acknowledgments

R.B. gratefully acknowledges to LPDP (Indonesia Endowment Fund for Education) BPI Program for the financial support of this work and the doctoral scholarship (KET-3/LPDP.3/2018).

## References

[1] Badri, A.F., Siregar, P.M.S.B.N., Palapa, N.R., Mohadi, R., Mardiyanto, M., Lesbani, A. (2021). Mg-Al/Biochar Composite with Stable Structure for Malachite Green Adsorption from Aqueous Solutions. *Bulletin of Chemical Reaction Engineering & Catalysis*, 16(1), 149–160. DOI: 10.9767/bcrec.16.1.10270.149-160.

[2] Chianese, S., Fenti, A., Iovino, P., Musmarra, D., Salvestrini, S. (2020). Sorption of Organic Pollutants by Humic Acids: A Review. *Molecules*, 25(4), 918. DOI: 10.3390/molecules25040918.

[3] Zhang, J. (2019). Physical insights into kinetic models of adsorption. *Separation and Purification Technology*, 229, 115832. DOI: 10.1016/j.seppur.2019.115832.

[4] Qiu, H., Lv, L., Pan, B.C., Zhang, Q.J., Zhang, W.M., Zhang, Q.X. (2009). Critical review in adsorption kinetic models. *Journal of Zhejiang University: Science A*, 10(5), 716–724. DOI: 10.1631/jzus.A0820524.

[5] Weber, W.J., Morris, J.C. (1963). Kinetics of adsorption on carbon from solution. *Journal of the Sanitary Engineering Division*, 89(2), 31–59. DOI: 10.1061/JSEDAI.0000430

[6] Largitte, L., Pasquier, R. (2016). A review of the kinetics adsorption models and their application to the adsorption of lead by an activated carbon. *Chemical Engineering Research and Design*, 109, 495–504. DOI: 10.1016/j.cherd.2016.02.006.

[7] Tan, I.A.W., Ahmad, A.L., Hameed, B.H. (2009). Adsorption isotherms, kinetics, thermodynamics and desorption studies of 2,4,6-trichlorophenol on oil palm empty fruit bunch-based activated carbon. *Journal of Hazardous Materials*, 164, 473–482. DOI: 10.1016/j.jhazmat.2008.08.025.

[8] Lagergren, S. (1898). Kungliga svenska vetenskapsakademiens. *Handlingar*, 24 (4), 1–39.

[9] Ho, Y.S., McKay, G. (1998). Sorption of dye from aqueous solution by peat. *Chemical Engineering Journal*, 70(2), 115–124. DOI: 10.1016/S1385-8947(98)00076-X.

[10] Ho, Y.S. (2006). Review of second-order models for adsorption systems. *Journal of Hazardous Materials*, 136(3), 681–689. DOI: 10.1016/j.jhazmat.2005.12.043.

[11] Robalds, A., Naja, G.M., Klavins, M. (2016). Highlighting inconsistencies regarding metal biosorption. *Journal of Hazardous Materials*, 304, 553–556. DOI: 10.1016/j.jhazmat.2015.10.042.

[12] Tran, H.N., You, S.J., Hosseini-Bandegharaei, A., Chao, H.P. (2017). Mistakes and inconsistencies regarding adsorption of contaminants from aqueous solutions: A critical review. *Water Research*, 120, 88–116. DOI: 10.1016/j.watres.2017.04.014.

[13] Azizian, S., Haerifar, M., Bashiri, H. (2009). Adsorption of methyl violet onto granular activated carbon: Equilibrium, kinetics and modeling. *Chemical Engineering Journal*, 146(1), 36–41. DOI: 10.1016/j.cej.2008.05.024.

[14] Santosa, S.J. (2014). Sorption kinetics of Cd(II) species on humic acid-based sorbent. *Clean - Soil, Air, Water*, 42(6), 760–766. DOI: 10.1002/clen.201200684.

[15] Rusdiarso, B., Basuki, R., Santosa, S.J. (2016). Evaluation of Lagergren kinetics equation by using novel kinetics expression of sorption of $Zn^{2+}$ onto horse dung humic acid (HD-HA). *Indonesian Journal of Chemistry*, 16(3), 338–346. DOI: 10.22146/ijc.1158.

[16] Basuki, R., Ngatijo, Santosa, S.J., Rusdiarso, B. (2018). Comparison the new kinetics equation of noncompetitive sorption Cd(II) and Zn(II) onto green sorbent horse dung humic acid (HD-HA). *Bulletin of Chemical Reaction Engineering & Catalysis*, 13(3), 475–488. DOI: 10.9767/bcrec.13.3.1774.475-488.

[17] Ngatijo, N., Basuki, R., Rusdiarso, B., Nuryono, N. (2020). Sorption-desorption profile of Au (III) onto silica modified quaternary amines (SMQA) in gold mining effluent. *Journal of Environmental Chemical Engineering*, 8(3), 103747. DOI: 10.1016/j.jece.2020.103747.

[18] Fang, D., Zhuang, X., Huang, L., Zhang, Q., Shen, Q., Jiang, L., Xu, X., Ji, F. (2020). Developing the new kinetics model based on the adsorption process: From fitting to comparison and prediction. *Science of the Total Environment*, 725(174), 138490. DOI: 10.1016/j.scitotenv.2020.138490.

[19] Hu, Q., Wang, Q., Feng, C., Zhang, Z., Lei, Z., Shimizu, K. (2018). Insights into mathematical characteristics of adsorption models and physical meaning of corresponding parameters. *Journal of Molecular Liquids*, 254, 20–25. DOI: 10.1016/j.molliq.2018.01.073.

[20] Kupeta, A.J.K., Naidoo, E.B., Ofomaja, A.E. (2018). Kinetics and equilibrium study of 2-nitrophenol adsorption onto polyurethane cross-linked pine cone biomass. *Journal of Cleaner Production*, 179, 191–209. DOI: 10.1016/j.jclepro.2018.01.034.

[21] Okoli, C.P., Ofomaja, A.E. (2018). Degree of time dependency of kinetic coefficient as a function of adsorbate concentration; new insights from adsorption of tetracycline onto monodispersed starch-stabilized magnetic nanocomposite. *Journal of Environmental Management*, 218, 139–147. DOI: 10.1016/j.jenvman.2018.04.060.

[22] Feng, X., Wang, P., Shi, Z., Kwon, K.D., Zhao, H., Yin, H., Lin, Z., Zhu, M., Liang, X., Liu, F., and Sparks, D.L. (2018). A Quantitative Model for the Coupled Kinetics of Arsenic Adsorption/Desorption and Oxidation on Manganese Oxides. *Environmental Science and Technology Letters*, 5(3), 175–180. DOI: 10.1021/acs.estlett.8b00058.

[23] Basuki, R., Rusdiarso, B., Santosa, S.J., Siswanta, D. (2021). Magnetite-Functionalized Horse Dung Humic Acid (HDHA) for the Uptake of Toxic Lead (II) from Artificial Wastewater. *Adsorption Science & Technology*, 2021(5523513), 1–15. DOI: 10.1155/2021/5523513

[24] Stevenson, F.J. (1994). *Humus Chemistry: Genesis, Composition, Reactions*. New York: John Wiley & Sons.

[25] No, H.K., Meyers, S.P., and Lee, K.S. (1989). Isolation and characterization of chitin from crawfish shell waste. *Journal of Agricultural and Food Chemistry*. 37(3), 575–579. DOI: 10.1021/jf00087a001

[26] Santosa, S.J., Siswanta, D., Sudiono, S., Utarianingrum, R. (2008). Chitin-humic acid hybrid as adsorbent for Cr(III) in effluent of tannery wastewater treatment. *Applied Surface Science*, 254(23), 7846–7850. DOI: 10.1016/j.apsusc.2008.02.102.

[27] Liu, J.F., Zhao, Z.S., Jiang, G. Bin (2008). Coating Fe3O4 magnetic nanoparticles with humic acid for high efficient removal of heavy metals in water. *Environmental Science and Technology*, 42(18), 6949–6954. DOI: 10.1021/es800924c.

[28] Santosa, S.J., Siswanta, D., Kurniawan, A., Rahmanto, W.H. (2007). Hybrid of chitin and humic acid as high performance sorbent for Ni(II). *Surface Science*, 601(22), 5155–5161. DOI: 10.1016/j.susc.2007.04.163.

[29] Abdou, E.S., Nagy, K.S.A., Elsabee, M.Z. (2008). Extraction and characterization of chitin and chitosan from local sources. *Bioresource Technology*, 99(5), 1359–1367. DOI: 10.1016/j.biortech.2007.01.051.

[30] Magnacca, G., Allera, A., Montoneri, E., Celi, L., Benito, D.E., Gagliardi, L.G., Gonzalez, M.C., Mártire, D.O., Carlos, L. (2014). Novel magnetite nanoparticles coated with waste-sourced biobased substances as sustainable and renewable adsorbing materials. *ACS Sustainable Chemistry and Engineering*, 2(6), 1518–1524. DOI: 10.1021/sc500213j.

[31] Tolesa, L.D., Gupta, B.S., Lee, M.J. (2019). Chitin and chitosan production from shrimp shells using ammonium-based ionic liquids. *International Journal of Biological Macromolecules*, 130, 818–826. DOI: 10.1016/j.ijbiomac.2019.03.018.

[32] Zarghani, M., Akhlaghinia, B. (2016). Magnetically separable Fe3O4@chitin as an eco-friendly nanocatalyst with high efficiency for green synthesis of 5-substituted-1H-tetrazoles under solvent-free conditions. *RSC Advances*, 6(38), 31850–31860. DOI: 10.1039/c6ra07252f.

[33] Koesnarpadi, S., Santosa, S.J., Siswanta, D., Rusdiarso, B. (2017). Humic Acid Coated Fe3O4 Nanoparticle for Phenol Sorption. *Indonesian Journal of Chemistry*, 17(2), 274–283. DOI: https://doi.org/10.22146/ijc.22545.

[34] Illés, E., Tombácz, E. (2006). The effect of humic acid adsorption on pH-dependent surface charging and aggregation of magnetite nanoparticles. *Journal of Colloid and Interface Science*, 295(1), 115–123. DOI: 10.1016/j.jcis.2005.08.003.

[35] Peng, L., Qin, P., Lei, M., Zeng, Q., Song, H., Yang, J., Shao, J., Liao, B., Gu, J. (2012). Modifying $Fe_3O_4$ nanoparticles with humic acid for removal of Rhodamine B in water. *Journal of Hazardous Materials*, 209–210, 193–198. DOI: 10.1016/j.jhazmat.2012.01.011.

[36] Jiang, W., Cai, Q., Xu, W., Yang, M., Cai, Y., Dionysiou, D.D., O'Shea, K.E. (2014). Cr(VI) adsorption and reduction by humic acid coated on magnetite. *Environmental Science and Technology*, 48(14), 8078–8085. DOI: 10.1021/es405804m.

[37] Rusdiarso, B., Basuki, R. (2020). Stability Improvement of Humic Acid as Sorbent through Magnetite and Chitin Modification. *Jurnal Kimia Sains dan Aplikasi*, 23(5), 152–159. DOI: 10.14710/jksa.23.5.152-159.

[38] Fu, Q., Hu, B., Zhou, X., Hu, Q., Sheng, J. (2016). Impact of key geochemical parameters on the attenuation of Pb(II) from water using a novel magnetic nanocomposite: fulvic acid-coated magnetite nanoparticles. *Desalination and Water Treatment*, 57(54), 26063–26072. DOI: 10.1080/19443994.2016.1157763.

[39] Anirudhan, T.S., Ramachandran, M. (2015). Adsorptive removal of basic dyes from aqueous solutions by surfactant modified bentonite clay (organoclay): Kinetic and competitive adsorption isotherm. *Process Safety and Environmental Protection*, 95, 215–225. DOI: 10.1016/j.psep.2015.03.003.

[40] Zehra, T., Lim, L.B.L., Priyantha, N. (2015). Removal behavior of peat collected from Brunei Darussalam for Pb(II) ions from aqueous solution: equilibrium isotherm, thermodynamics, kinetics and regeneration studies. *Environmental Earth Sciences*, 74(3), 2541–2551. DOI: 10.1007/s12665-015-4273-2.

[41] Liu, Y., Li, T., Zeng, G., Zheng, B., Xu, W., Liu, S. (2016). Removal of Pb(II) from aqueous solution by magnetic humic acid/chitosan composites. *Journal of Central South University*, 23(11), 2809–2817. DOI: 10.1007/s11771-016-3344-1.

[42] Chen, R.P., Zhang, Y.L., Wang, X.Y., Zhu, C.Y., Ma, A.J., Jiang, W.M. (2015). Removal of methylene blue from aqueous solution using humic-acid coated magnetic nanoparticles. *Desalination and Water Treatment*, 55(2), 539–548. DOI: 10.1080/19443994.2014.916233.

[43] Santosa, S.J., Kunarti, E.S., Aprilita, N.H., Wulandari, B., Bawani, D.N. (2019). Sorption mechanism and performance of peat soil humin for Methylene blue and p-Nitrophenol. *Indonesian Journal of Chemistry*, 19(1), 198–210. DOI: 10.22146/ijc.33635.

[44] Liu, S. (2015). Cooperative adsorption on solid surfaces. *Journal of Colloid and Interface Science*, 450, 224–238. DOI: 10.1016/j.jcis.2015.03.013.

[45] Chakravorti, R.K. and Weber, T.W. (1974). Pore and Solid Diffusion Models for fixed-bed adsorbers. *AIChE Journal*, 20(2), 228-238. DOI: 10.1002/aic.690200204.

[46] Freundlich, H. (1906). Über die Adsorption in Lösungen. *Zeitschrift für Physikalische Chemie*, 57U(1), 385–470. DOI: 10.1515/zpch-1907-5723.

[47] Tempkin, M.I., Pyzhev, V. (1940). Kinetics of ammonia synthesis on promoted iron catalyst. *Acta Phys. Chim. USSR*, 12(1), 327–356.

[48] Uddin, M.K., Nasar, A. (2020). Walnut shell powder as a low-cost adsorbent for methylene blue dye: isotherm, kinetics, thermodynamic, desorption and response surface methodology examinations. *Scientific Reports*, 10(1), 1–13. DOI: 10.1038/s41598-020-64745-3.

[49] Shen, S., Pan, T., Liu, X., Yuan, L., Zhang, Y., Wang, J., Guo, Z. (2010). Adsorption of Pd(II) complexes from chloride solutions obtained by leaching chlorinated spent automotive catalysts on ion exchange resin Diaion WA21J. *Journal of Colloid and Interface Science*, 345(1), 12–18. DOI: 10.1016/j.jcis.2010.01.049.

[50] Araújo, C.S.T., Almeida, I.L.S., Rezende, H.C., Marcionilio, S.M.L.O., Léon, J.J.L., de Matos, T.N. (2018). Elucidation of mechanism involved in adsorption of Pb(II) onto lobeira fruit (*Solanum lycocarpum*) using Langmuir, Freundlich and Temkin isotherms. *Microchemical Journal*, 137, 348–354. DOI: 10.1016/j.microc.2017.11.009.

[51] Duran, C., Ozdes, D., Gundogdu, A., Senturk, H.B. (2011). Kinetics and isotherm analysis of basic dyes adsorption onto almond shell (Prunus dulcis) as a low cost adsorbent. *Journal of Chemical and Engineering Data*, 56(5), 2136–2147. DOI: 10.1021/je101204j.

[52] Alghamdi, A.A., Al-Odayni, A.B., Abduh, N.A.Y., Alramadhan, S.A., Aljboar, M.T., Saeed, W.S. (2021). Adsorptive Performance of Polypyrrole-Based KOH-Activated Carbon for the Cationic Dye Crystal Violet: Kinetic and Equilibrium Studies. *Adsorption Science and Technology*, 2021 (5527594), 1-11. DOI: 10.1155/2021/5527594.

[53] Tan, I.A.W., Ahmad, A.L., Hameed, B.H. (2008). Adsorption of basic dye on high-surface-area activated carbon prepared from coconut husk: Equilibrium, kinetic and thermodynamic studies. *Journal of Hazardous Materials*, 154(1–3), 337–346. DOI: 10.1016/j.jhazmat.2007.10.031.

[54] Duval, J.F.L., Van Leeuwen, H.P. (2012). Rates of ionic reactions with charged nanoparticles in aqueous media. *Journal of Physical Chemistry A*, 116(25), 6443–6451. DOI: 10.1021/jp209488v.

[55] Town, R.M., Van Leeuwen, H.P., Buffle, J. (2012). Chemodynamics of soft nanoparticulate complexes: Cu(II) and Ni(II) complexes with fulvic acids and aquatic humic acids. *Environmental Science and Technology*, 46(19), 10487–10498. DOI: 10.1021/es3018013.

[56] Sabarinathan, C., Karuppasamy, P., Vijayakumar, C.T., Arumuganathan, T. (2019). Development of methylene blue removal methodology by adsorption using molecular polyoxometalate: Kinetics, Thermodynamics and Mechanistic Study. *Microchemical Journal*, 146, 315–326. DOI: 10.1016/j.microc.2019.01.015.

[57] Almeida, C.A.P., Debacher, N.A., Downs, A.J., Cottet, L., Mello, C.A.D. (2009). Removal of methylene blue from colored effluents by adsorption on montmorillonite clay. *Journal of Colloid and Interface Science*, 332(1), 46–53. DOI: 10.1016/j.jcis.2008.12.012.

[58] Agarwal, S., Rani, A. (2017). Adsorption of resorcinol from aqueous solution onto CTAB/NaOH/flyash composites: Equilibrium, kinetics and thermodynamics. *Journal of Environmental Chemical Engineering*, 5(1), 526–538. DOI: 10.1016/j.jece.2016.11.035.

[59] Sari, A.A., Amriani, F., Muryanto, M., Triwulandari, E., Sudiyani, Y., Barlianti, V., Narrij Lotulung, P.D., Hadibarata, T. (2017). Mechanism, adsorption kinetics and applications of carbonaceous adsorbents derived from black liquor sludge. *Journal of the Taiwan Institute of Chemical Engineers*, 77, 236–243. DOI: 10.1016/j.jtice.2017.05.008.

[60] Gunasundari, E., Kumar, P.S. (2017). Adsorption isotherm, kinetics and thermodynamic analysis of Cu(II) ions onto the dried algal biomass (Spirulina platensis). *Journal of Industrial and Engineering Chemistry*, 56, 129–144. DOI: 10.1016/j.jiec.2017.07.005.

[61] Stähelin, P.M., Valério, A., Guelli Ulson de Souza, S.M. de A., da Silva, A., Borges Valle, J.A., Ulson de Souza, A.A. (2018). Benzene and toluene removal from synthetic automotive gasoline by mono and bicomponent adsorption process. *Fuel*, 231, 45–52. DOI: 10.1016/j.fuel.2018.04.169.

[62] Darwish, A.A.A., Rashad, M., AL-Aoh, H.A. (2019). Methyl orange adsorption comparison on nanoparticles: Isotherm, kinetics, and thermodynamic studies. *Dyes and Pigments*, 160, 563–571. DOI: 10.1016/j.dyepig.2018.08.045.

[63] Marczewski, A.W. (2010). Application of mixed order rate equations to adsorption of methylene blue on mesoporous carbons. *Applied Surface Science*, 256(17), 5145–5152. DOI: 10.1016/j.apsusc.2009.12.078.

[64] Guo, X., Wang, J. (2019). A general kinetic model for adsorption: Theoretical analysis and modeling. *Journal of Molecular Liquids*, 288, 111100. DOI: 10.1016/j.molliq.2019.111100.

[65] Wang, J., Guo, X. (2020). Adsorption kinetic models: Physical meanings, applications, and solving methods. *Journal of Hazardous Materials*, 390, 122156. DOI: 10.1016/j.jhazmat.2020.122156.

[66] Ho, Y.S., McKay, G. (1998). The kinetics of sorption of basic dyes from aqueous solution by sphagnum moss peat. *The Canadian Journal of Chemical Engineering*, 76(4), 822–827. DOI: 10.1002/cjce.5450760419.

[67] Azizian, S. (2004). Kinetic models of sorption: A theoretical analysis. *Journal of Colloid and Interface Science*, 276(1), 47–52. DOI: 10.1016/j.jcis.2004.03.048.

[68] Kalavathy, M.H., Karthikeyan, T., Rajgopal, S., Miranda, L.R. (2005). Kinetic and isotherm studies of Cu(II) adsorption onto H3PO 4-activated rubber wood sawdust. *Journal of Colloid and Interface Science*, 292(2), 354–362. DOI: 10.1016/j.jcis.2005.05.087.

[69] Li, Y., Yue, Q., Gao, B. (2010). Adsorption kinetics and desorption of Cu ( II ) and Zn ( II ) from aqueous solution onto humic acid. *Journal of Hazardous Materials*, 178(1–3), 455–461. DOI: 10.1016/j.jhazmat.2010.01.103.

[70] Lu, S., Liu, W., Wang, Y., Zhang, Y., Li, P., Jiang, D., Fang, C., Li, Y. (2019). An adsorbent based on humic acid and carboxymethyl cellulose for efficient dye removal from aqueous solution. *International Journal of Biological Macromolecules*, 135, 790–797. DOI: 10.1016/j.ijbiomac.2019.05.095.

[71] Zhang, X., Zhang, P., Wu, Z., Zhang, L., Zeng, G., Zhou, C. (2013). Adsorption of methylene blue onto humic acid-coated Fe3O4 nanoparticles. *Colloids and Surfaces A: Physicochemical and Engineering Aspects*, 435, 85–90. DOI: 10.1016/j.colsurfa.2012.12.056.

[72] Luo, W.J., Gao, Q., Wu, X.L., Zhou, C.G. (2014). Removal of Cationic Dye (Methylene Blue) from Aqueous Solution by Humic Acid-Modified Expanded Perlite: Experiment and Theory. *Separation Science and Technology (Philadelphia)*, 49(15), 2400–2411. DOI: 10.1080/01496395.2014.920395.

[73] Isloor, A.M., Shenvi, S.S., Ismail, A.F., Shilton, S.J. (2015). Humic Acid Based Biopolymeric Membrane for Effective Removal of Methylene Blue and Rhodamine B. *Industrial & Engineering Chemistry Research*, 54(18), 4965–4975. DOI: 10.1021/acs.iecr.5b00761.

[74] Inam, E., Udo, O.O., Edet, J.B., Etim, U.J., Offiong, N.O. (2018). Adsorption of Methylene Blue from Aqueous Solution by Humic Acid Extracted from Freshwater River Humus. *J. Mater. Environ. Sci.*, 9(4), 1324–1334. [Online]. Available: https://www.jmaterenvironsci.com/Document/vol9/vol9_N4/145-JMES-2706-Inam.pdf.

[75] Bartczak, P., Norman, M., Klapiszewski, L., Karwańska, N., Kawalec, M., Baczyńska, M., Wysokowski, M., Zdarta, B., Ciesielczyk, F., Jesionowski, T. (2018). Removal of nickel(II) and lead(II) ions from aqueous solution using peat as a low-cost adsorbent: A kinetic and equilibrium study. *Arabian Journal of Chemistry*, 11(8), 1209–1222. DOI: 10.1016/j.arabjc.2015.07.018.

[76] Chen, R., Zhang, Y., Shen, L., Wang, X., Chen, J., Ma, A., Jiang, W. (2015). Lead(II) and methylene blue removal using a fully biodegradable hydrogel based on starch immobilized humic acid. *Chemical Engineering Journal*, 268, 348–355. DOI: 10.1016/j.cej.2015.01.081.

[77] Kushwaha, A., Rani, R., Patra, J.K. (2020). Adsorption kinetics and molecular interactions of lead [Pb(II)] with natural clay and humic acid. *International Journal of Environmental Science and Technology*, 17(3), 1325–1336. DOI: 10.1007/s13762-019-02411-6.

[78] Basu, H., Saha, S., Mahadevan, I.A., Pimple, M.V., Singhal, R.K. (2019). Humic acid coated cellulose derived from rice husk: A novel biosorbent for the removal of Ni and Cr. *Journal of Water Process Engineering*, 32, 100892. DOI: 10.1016/j.jwpe.2019.100892.

## APPENDICES

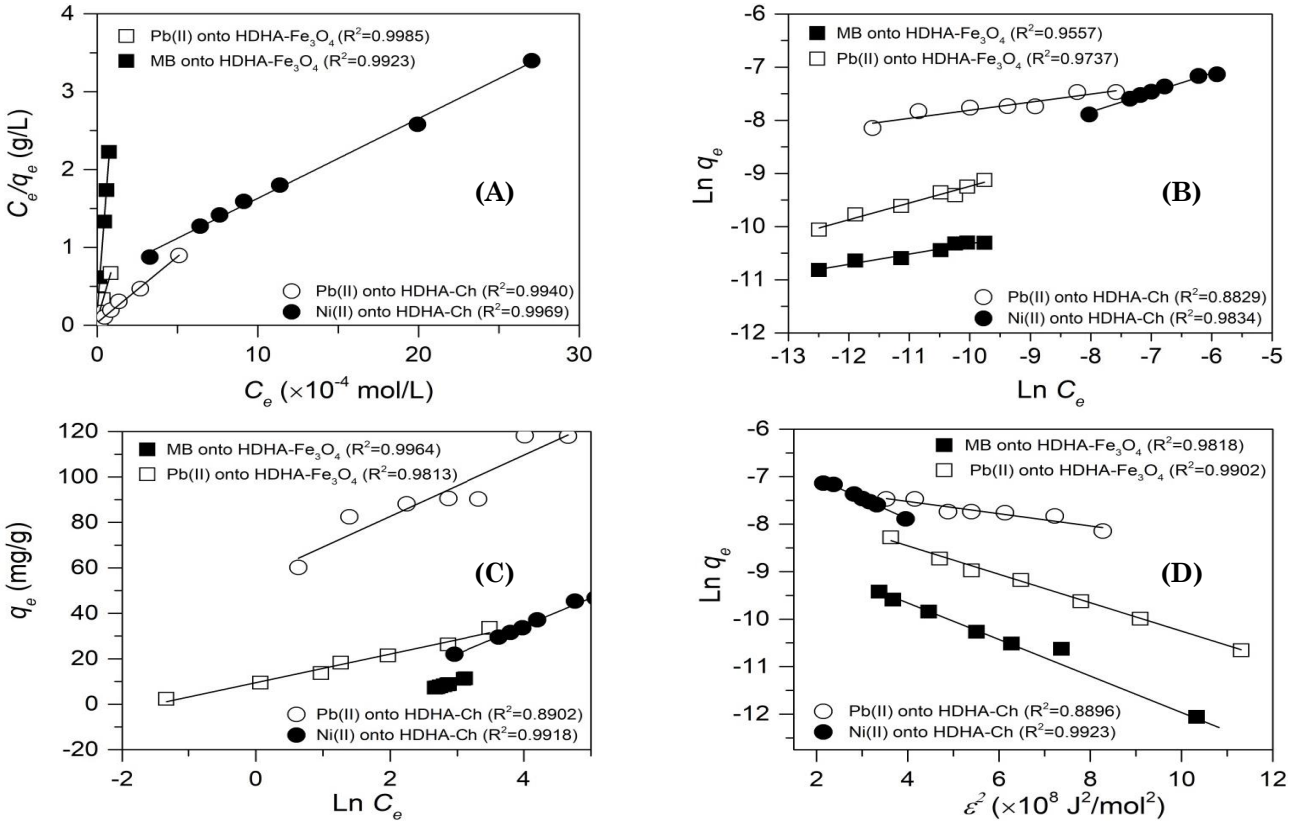


Figure S1. The plot of equilibrium data of adsorbed Pb(II)-Ni(II) onto HDHA-Ch and Pb(II)-MB onto HDHA $Fe_3O_4$ on linearized adsorption isotherm models: the Langmuir (A), Freundlich (B), Temkin (C), and D-R (D)

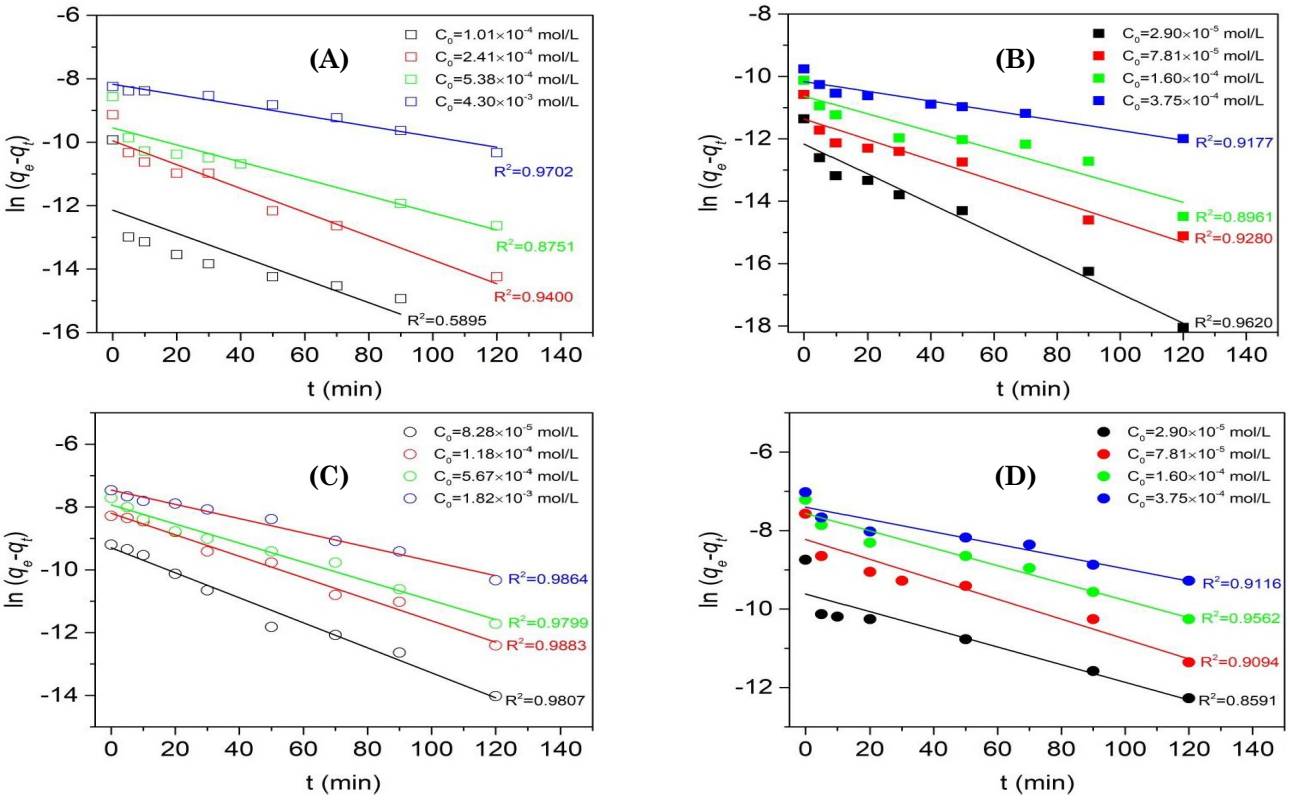


Figure S2. The plot of kinetics data of adsorbed (A) Pb(II) onto HDHA-$Fe_3O_4$; (B) MB onto HDHA-$Fe_3O_4$; (C) Pb(II) onto HDHA-Ch; and (D) Ni(II) onto HDHA-Ch on linearized Lagergren's kinetics model

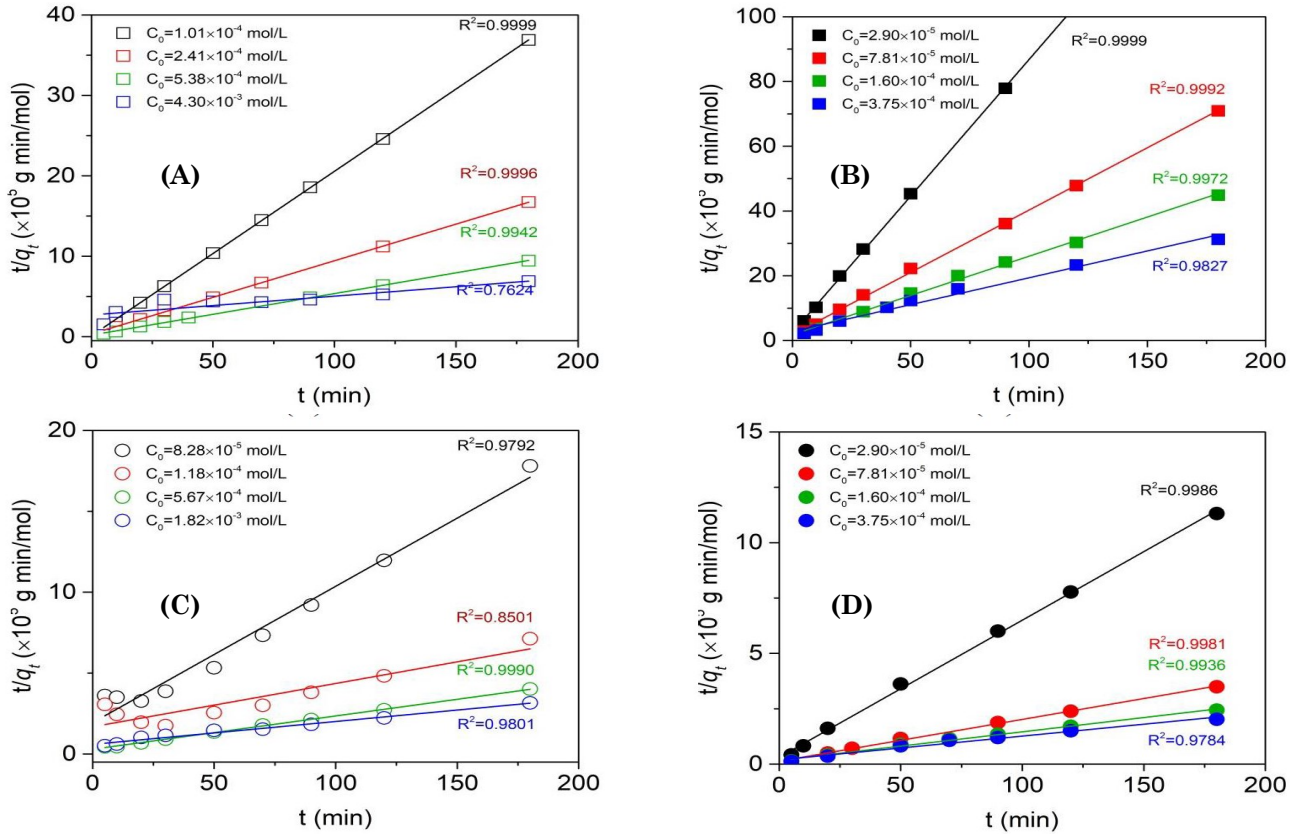


Figure S3. The plot of kinetics data of adsorbed (A) Pb(II) onto HDHA-$Fe_3O_4$; (B) MB onto HDHA-$Fe_3O_4$; (C) Pb(II) onto HDHA-Ch; and (D) Ni(II) onto HDHA-Ch on linearized Ho's kinetics model.

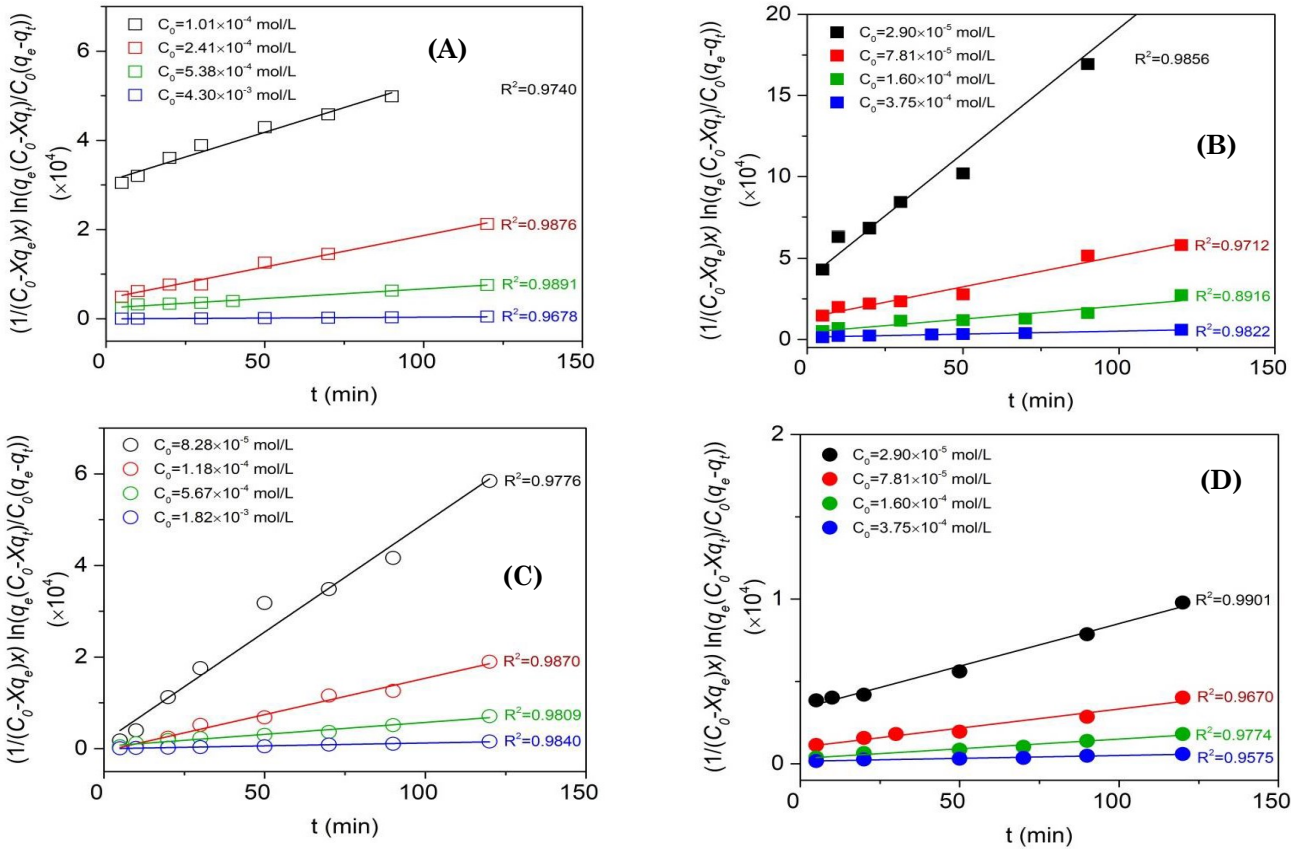


Figure S4. The plot of kinetics data of adsorbed (A) Pb(II) onto HDHA-$Fe_3O_4$; (B) MB onto HDHA-$Fe_3O_4$; (C) Pb(II) onto HDHA-Ch; and (D) Ni(II) onto HDHA-Ch on linearized Santosa's kinetics model.

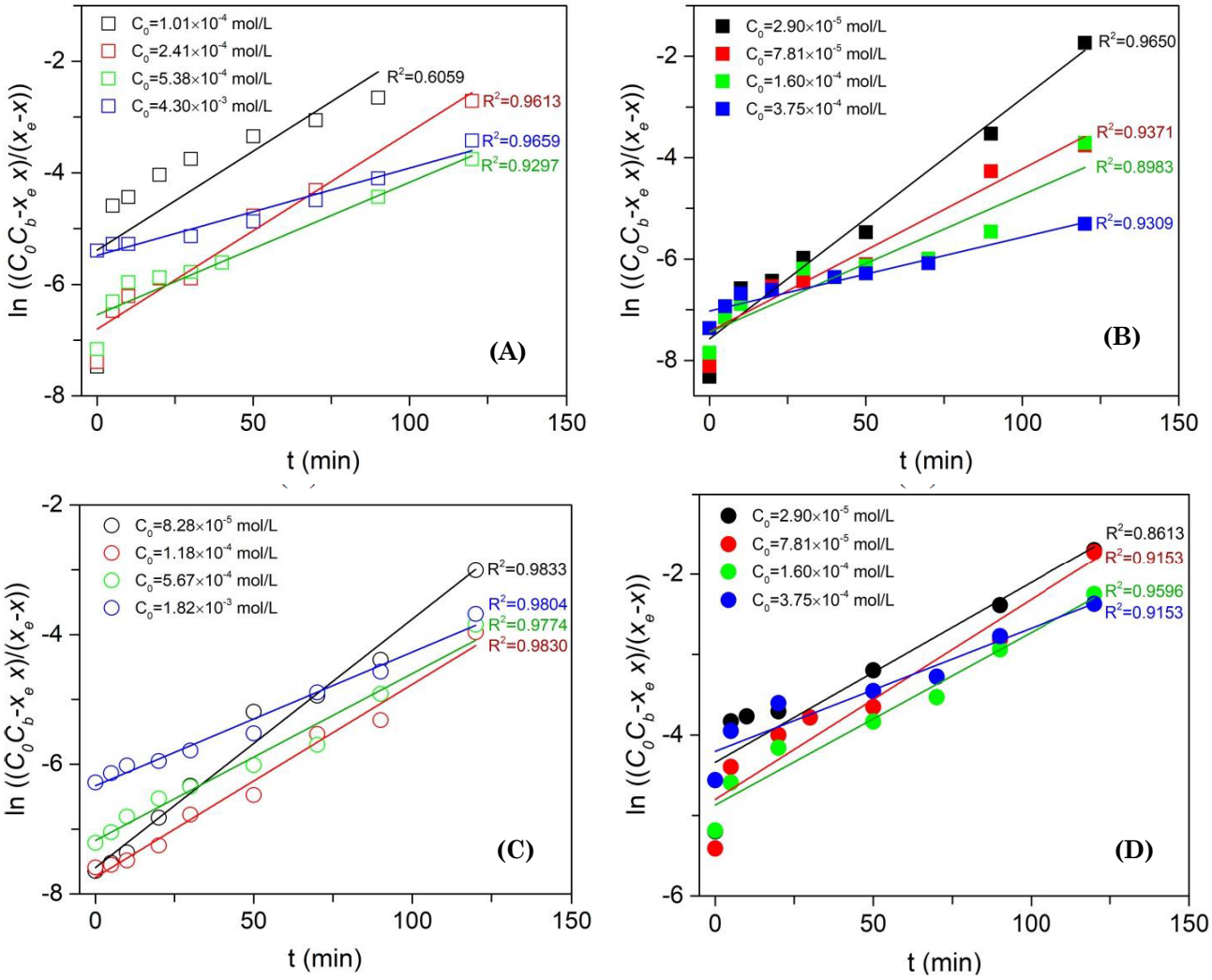


Figure S5 The plot of kinetics data of adsorbed (A) Pb(II) onto HDHA-$Fe_3O_4$; (B) MB onto HDHA-$Fe_3O_4$; (C) Pb(II) onto HDHA-Ch; and (D) Ni(II) onto HDHA-Ch on linearized RBS's kinetics model.

Table S1. Corresponding parameters obtained from linearized Lagergren, Ho, Santosa, and RBS kinetics model of Pb(II)-MB onto HDHA-$Fe_3O_4$ and Pb(II)-Ni(II) onto HDHA-Ch.

| **Models** | | | **Pb(II) onto HDHA-$Fe_3O_4$** | | | | **MB onto HDHA-$Fe_3O_4$** | | | | | |
|---|---|---|---|---|---|---|---|---|---|---|---|---|
| Lagergren | $C_0$ (mg/L) | Exp. $q_e$ ($\times10^{-5}$ mol/g) | Calc. $q_e$ ($\times10^{-5}$ mol/g) | $k_{Lag}$ ($min^{-1}$) | $k_d$ | $R^2$ | $C_0$ (mg/L) | Exp. $q_e$ ($\times10^{-5}$ mol/g) | Calc. $q_e$ ($\times10^{-5}$ mol/g) | $k_{Lag}$ ($min^{-1}$) | $k_d$ | $R^2$ |
| | 20 | 4.88 | 0.53 | 0.037 | - | 0.5895 | 10 | 1.16 | 0.52 | 0.048 | - | 0.9620 |
| | 50 | 10.76 | 4.74 | 0.038 | - | 0.9400 | 25 | 2.54 | 1.16 | 0.033 | - | 0.9280 |
| | 100 | 19.08 | 7.13 | 0.027 | - | 0.8751 | 50 | 4.01 | 2.41 | 0.028 | - | 0.8961 |
| | 400 | 26.09 | 28.23 | 0.017 | - | 0.9702 | 100 | 5.77 | 3.85 | 0.016 | - | 0.9177 |
| Ho | $C_0$ (mg/L) | Exp. $q_e$ ($\times10^{-5}$ mol/g) | Calc. $q_e$ ($\times10^{-5}$ mol/g) | $k_{Ho}$ (g $mol^{-1}$ $min^{-1}$) | $k_d$ | $R^2$ | $C_0$ (mg/L) | Exp. $q_e$ ($\times10^{-5}$ mol/g) | Calc. $q_e$ ($\times10^{-5}$ mol/g) | $k_{Ho}$ (g $mol^{-1}$ $min^{-1}$) | $k_d$ | $R^2$ |
| | 20 | 4.88 | 4.89 | 34397.26 | - | 0.9999 | 10 | 1.16 | 1.19 | 29784.96 | - | 0.9999 |
| | 50 | 10.76 | 10.99 | 2363.68 | - | 0.9996 | 25 | 2.54 | 2.60 | 8301.59 | - | 0.9992 |
| | 100 | 19.08 | 19.40 | 1268.01 | - | 0.9942 | 50 | 4.01 | 4.13 | 3248.16 | - | 0.9972 |
| | 400 | 26.09 | 42.78 | 20.18 | - | 0.7624 | 100 | 5.77 | 6.03 | 983.33 | - | 0.9827 |
| Santosa | $C_0$ (mg/L) | Exp. $q_e$ ($\times10^{-5}$ mol/g) | Calc. $q_e$ | $k_s$ ($(mol/L)^{-1}$ $min^{-1}$) | $k_{ds}$ ($\times10^{-2}$ $min^{-1}$) | $R^2$ | $C_0$ (mg/L) | Exp. $q_e$ ($\times10^{-5}$ mol/g) | $k_s$ ($(mol/L)^{-1}$ $min^{-1}$) | Calc. $q_e$ | $k_{ds}$ ($\times10^{-2}$ $min^{-1}$) | $R^2$ |
| | 20 | 4.88 | - | 221.8 | - | 0.9740 | 10 | 1.16 | 1541.90 | - | - | 0.9856 |
| | 50 | 10.76 | - | 141.29 | - | 0.9876 | 25 | 2.54 | 381.68 | - | - | 0.9712 |
| | 100 | 19.08 | - | 42.75 | 2.29 | 0.9891 | 50 | 4.01 | 161.5 | - | 2.58 | 0.8916 |
| | 400 | 26.09 | - | 3.94 | 1.69 | 0.9678 | 100 | 5.77 | 36.85 | - | 1.38 | 0.9822 |
| RBS | $C_0$ (mg/L) | Exp. $q_e$ ($\times10^{-5}$ mol/g) | Calc. $q_e$ ($\times10^{-5}$ mol/g) | $k_{RBS}$ ($(mol/L)^{-1}$ $min^{-1}$) | $k_d$ ($\times10^{-3}$ $min^{-1}$) | $R^2$ | $C_0$ (mg/L) | Exp. $q_e$ ($\times10^{-5}$ mol/g) | Calc. $q_e$ ($\times10^{-5}$ mol/g) | $k_{RBS}$ ($(mol/L)^{-1}$ $min^{-1}$) | $k_d$ ($\times10^{-3}$ $min^{-1}$) | $R^2$ |
| | 20 | 4.88 | 0.61 | 75.4 | 1.12 | 0.6059 | 10 | 1.16 | 0.55 | 215.73 | 9.05 | 0.9650 |
| | 50 | 10.76 | 5.98 | 87.91 | 3.55 | 0.9613 | 25 | 2.54 | 1.28 | 128.52 | 10.00 | 0.9731 |
| | 100 | 19.08 | 10.29 | 60.13 | 4.16 | 0.9297 | 50 | 4.01 | 2.67 | 87.44 | 10.04 | 0.8983 |
| | 400 | 26.09 | 28.39 | 3.91 | 0.81 | 0.9659 | 100 | 5.77 | 4.12 | 28.08 | 5.06 | 0.9309 |
| **Models** | | | **Pb(II) onto HDHA-Ch** | | | | **Ni(II) onto HDHA-Ch** | | | | | |
| Lagergren | $C_0$ (mg/L) | Exp. $q_e$ ($\times10^{-5}$ mol/g) | Calc. $q_e$ ($\times10^{-5}$ mol/g) | $k_{Lag}$ ($min^{-1}$) | $k_d$ | $R^2$ | $C_0$ (mg/L) | Exp. $q_e$ ($\times10^{-5}$ mol/g) | Calc. $q_e$ ($\times10^{-5}$ mol/g) | $k_{Lag}$ ($min^{-1}$) | $k_d$ | $R^2$ |
| | 20 | 10.11 | 9.16 | 0.040 | - | 0.9807 | 20 | 15.92 | 6.67 | 0.023 | - | 0.8591 |
| | 50 | 25.27 | 27.84 | 0.034 | - | 0.9883 | 50 | 51.49 | 26.77 | 0.026 | - | 0.9094 |
| | 100 | 44.84 | 35.92 | 0.030 | - | 0.9799 | 100 | 73.73 | 42.79 | 0.022 | - | 0.9562 |
| | 400 | 57.07 | 57.64 | 0.023 | - | 0.9864 | 400 | 88.94 | 60.89 | 0.016 | - | 0.9116 |
| Ho | $C_0$ (mg/L) | Exp. $q_e$ ($\times10^{-5}$ mol/g) | Calc. $q_e$ ($\times10^{-5}$ mol/g) | $k_{Ho}$ (g $mol^{-1}$ $min^{-1}$) | $k_d$ | $R^2$ | $C_0$ (mg/L) | Exp. $q_e$ ($\times10^{-5}$ mol/g) | Calc. $q_e$ ($\times10^{-5}$ mol/g) | $k_{Ho}$ (g $mol^{-1}$ $min^{-1}$) | $k_d$ | $R^2$ |
| | 20 | 10.11 | 11.87 | 365.89 | - | 0.9792 | 20 | 15.92 | 16.15 | 1247.31 | - | 0.9986 |
| | 50 | 25.27 | 37.39 | 42.4 | - | 0.8501 | 50 | 51.49 | 52.99 | 267.58 | - | 0.9981 |
| | 100 | 44.84 | 48.62 | 141.99 | - | 0.9990 | 100 | 73.73 | 77.54 | 97.80 | - | 0.9936 |
| | 400 | 57.07 | 70.74 | 33.39 | - | 0.9801 | 400 | 88.94 | 93.13 | 59.65 | - | 0.9784 |
| Santosa | $C_0$ (mg/L) | Exp. $q_e$ ($\times10^{5}$ mol/g) | Calc. $q_e$ | $k_s$ ($(mol/L)^{-1}min^{-1}$) | $k_{ds}$ ($\times10^{-5}$ $min^{-1}$) | $R^2$ | $C_0$ (mg/L) | Exp. $q_e$ ($\times10^{-5}$ mol/g) | Calc. $q_e$ | $k_s$ ($(mol/L)^{-1}$ $min^{-1}$) | $k_{ds}$ ($\times10^{-2}$ $min^{-1}$) | $R^2$ |
| | 20 | 10.11 | - | 477.95 | - | 0.9776 | 20 | 15.92 | - | 51.74 | - | 0.9901 |
| | 50 | 25.27 | - | 159.02 | - | 0.9870 | 50 | 51.49 | - | 23.22 | - | 0.9670 |
| | 100 | 44.84 | - | 52.18 | - | 0.9809 | 100 | 73.73 | - | 11.78 | 1.99 | 0.9774 |
| | 400 | 57.07 | - | 12.49 | 1.02 | 0.9840 | 400 | 88.94 | - | 2.44 | 1.33 | 0.9575 |
| RBS | $C_0$ (mg/L) | Exp. $q_e$ ($\times10^{-5}$ mol/g) | Calc. $q_e$ ($\times10^{-5}$ mol/g) | $k_{RBS}$ ($(mol/L)^{-1}$ $min^{-1}$) | $k_d$ ($\times10^{-4}$ $min^{-1}$) | $R^2$ | $C_0$ (mg/L) | Exp. $q_e$ ($\times10^{-5}$ mol/g) | Calc. $q_e$ ($\times10^{-5}$ mol/g) | $k_{RBS}$ ($(mol/L)^{-1}$ $min^{-1}$) | $k_d$ ($\times10^{-3}$ $min^{-1}$) | $R^2$ |
| | 20 | 10.11 | 9.62 | 96.26 | 8.71 | 0.9833 | 20 | 15.92 | 2.70 | 4.15 | 138.85 | 0.8613 |
| | 50 | 25.27 | 29.48 | 98.48 | 20.67 | 0.9830 | 50 | 51.49 | 11.21 | 6.13 | 122.17 | 0.9153 |
| | 100 | 44.84 | 43.34 | 67.56 | 42.74 | 0.9774 | 100 | 73.73 | 21.53 | 4.27 | 108.71 | 0.9596 |
| | 400 | 57.07 | 59.99 | 14.58 | 4.91 | 0.9804 | 400 | 88.94 | 24.92 | 1.57 | 8.47 | 0.9153 |